

The Radio Structure of 45 Quasars at $z < 1.5$

V. K. Kapahi *National Centre for Radio Astrophysics, Tata Institute of Fundamental Research, Poona University Campus, Pune 411007, India*

Received 1995 January 3; accepted 1995 January 11.

Abstract. Radio maps at 5 GHz with an angular resolution of 1 to 2 arcsec and a dynamic range $\gtrsim 200:1$ are presented for a sample of 45 radio quasars at redshifts between 0.2 and 1.5. The sources were imaged from observations made with the Very Large Array with the aim of investigating the epoch dependence of misalignments and asymmetries in their extended radio structure. Maps of some of the larger radio sources are presented also at a frequency of 1.5 GHz with a typical angular resolution of ~ 4 arcsec. The radio structure of most of the quasars reported here has been delineated in considerably greater detail than available in the literature.

Key words: Quasars—active galactic nuclei—radio structure.

1. Introduction

Radio quasars are among the most distant and energetic extragalactic objects known in the Universe. In the three decades since their discovery, a variety of observational and theoretical studies of their radio emission has provided a considerable body of information and insight into the processes responsible for their workings. While the source of their enormous energy output is widely believed to result ultimately from the gravitational energy associated with the collapse of super massive black holes, the overall double radio structure with characteristic features such as hot spots, lobes and bridges or tails is attributed to the propagation of twin jets from the central engine and their interaction with the ambient interstellar and intergalactic medium surrounding the objects. Observations of radio quasars at different redshifts also provide an important source of information on the evolution with epoch in the physical conditions both inside and outside their parent galaxies.

Although the extended structure of most radio quasars is generally fairly symmetric, with the hot spots on the two sides being almost collinear with the radio core and roughly equidistant from it, a sizeable fraction of quasars are now known to show significant departures from symmetry and collinearity (e.g. Hintzen *et al.* 1983; Barthel *et al.* 1988). Several mechanisms have been invoked to explain such asymmetries and misalignments, such as: light travel time differences from the two hot spots; intrinsically asymmetric ejections; ejection only on one side at a time; motion of the quasar in a cluster; precession of the central engine; gravitational lensing effects; bending of jets by interstellar or intergalactic gas clouds etc. From a study of the misalignments at different cosmic epochs, it was reported by Barthel & Miley (1988) that the extended emission appeared much more bent and distorted at high redshifts ($z \gtrsim 1.5$) than at lower redshifts. They considered the jet-cloud interaction to be the most plausible

explanation for the effect and regarded this as evidence for a clumpier intergalactic medium at earlier epochs.

In view of the cosmological significance of the above mentioned result, it is important to confirm the increase in misalignments with redshift and to rule out the possibility of any instrumental or observational selection effects being responsible for the effect. This is particularly important because the effect appears to become important mainly at $z \geq 1.5$, which was also the dividing redshift between two samples of quasars used by Barthel & Miley (1988) to investigate the epoch dependence of misalignments. While the structures of almost all the 80 objects in their high- z ($z > 1.5$) sample were determined by Barthel *et al.* (1988) using the Very Large Array with a high angular resolution of ~ 0.4 arcsec and a dynamic range generally exceeding $\sim 200:1$, the data for most of their comparison sample of about 40 quasars at $z < 1.5$ were taken from maps available in the literature that had been made with much poorer angular resolutions and dynamic ranges, mostly with the Cambridge 1m array (e.g. Riley & Pooley 1975) or with the Westerbork Synthesis Radio Telescope (Miley & Hartsuijker 1978).

The observations reported in the present paper were undertaken primarily to map the extended structure of a larger sample of quasars at low redshifts ($z < 1.5$) with higher angular resolution and dynamic range than available in the literature in order to carry out a better comparison of the radio structures at different redshifts. A sample of 45 quasars was mapped using the VLA at a frequency of 5 GHz. The resulting radio images and the values of some derived parameters are presented here. The sample selection and observations are described in section 2 and the results presented in section 3.

Preliminary results of an investigation of the epoch dependence of misalignments based on the data presented here and available in the literature have been presented earlier (Kapahi 1990). A detailed analysis together with a comparison of the quasar data with similar data on samples of radio galaxies will be reported in a subsequent publication.

2. Sample selection and observations

While enlarging the low- z quasar sample it was important to keep in mind the criteria used to form the high- z sample in order to minimize the effect on the structures due to factors other than the redshift. The following criteria were employed to select the sources to be mapped with VLA.

- i. $z < 1.5$
- ii. Steep radio spectra, with spectral index $\alpha_{1.4\text{ GHz}}^{5\text{ GHz}} \geq 0.6$. (defined such that $S(\nu) \propto \nu^{-\alpha}$. This criterion was used by BM to form the high- z sample and ensures that the samples do not contain core-dominated quasars which may have their jet axes close to the observer's line of sight as suggested by quasar unification schemes based on the relativistic beaming effects in the nuclear jets (Kapahi & Saikia 1982; Orr & Browne 1982).
- iii. Known to have extended radio structure with angular sizes ≥ 4 arcsec. This was to ensure at least a few beam sizes over the radio extent in order to determine the misalignments with reasonable confidence.

- iv. High radio luminosity; $P(5\text{GHz}) > 10^{26} \text{WHz}^{-1}$, assuming $q_0 = 0.5$ and $H_0 = 75 \text{kms}^{-1} \text{Mpc}^{-1}$. This is also the minimum luminosity in the high- z sample.

The sample of sources selected for observations was drawn up starting from the compilation of known extended steep-spectrum quasars (Singal 1988) and essentially picking all those that satisfied the criteria (i) to (iii) listed above and in addition had a flux density $\gtrsim 2 \text{Jy}$ at 400 MHz (to ensure that criterion (iv) is also satisfied) and did not already have radio maps with high angular resolution ($\sim 1\text{--}2 \text{arcsec}$) and dynamic range ($\gtrsim 200$) available in the literature.

The 45 quasars selected by the above criteria for observations with the VLA had a median redshift of ~ 0.7 which is about 2.5 times smaller than the median z in the high- z sample of Barthel and Miley. Because the median angular size of radio quasars is known to decrease roughly linearly with increasing z (e.g. Kapahi 1987), a typical angular resolution of $\sim 1 \text{arcsec}$ was necessary for the low- z sources to have a similar number of resolution elements across their total extent on average as was available for the maps of the high- z quasars which had an angular resolution of $\sim 0.4 \text{arcsec}$. It was therefore decided to map the 45 sources at a frequency of 5 GHz in the ‘‘B’’ configuration of VLA which provides a resolution of $\sim 1 \text{arcsec}$. As observations in this configuration are not very sensitive to structure on a scale $\gtrsim 30 \text{arcsec}$ it was decided to observe some of the larger sources in the sample at the lower frequency of 1.5 GHz (in the same ‘‘B’’ configuration) as well.

The observations were made on 18 March 1989 during a continuous run of about 15 hours. Each source was observed for a duration of about 5 to 8 minutes at each of two hour angles. A phase calibrator was observed typically every 30 minutes. The flux calibration was carried out using 3C48. The observations in the 6 cm band had an effective bandwidth of 100 MHz centred at 4.86 GHz while those in the 20 cm band had a bandwidth of 100 MHz centred at 1.54 GHz.

3. Data reduction and results

The data were mostly processed at the Array Operations Centre of NRAO at Socorro, USA, using the standard AIPS software. After calibration and editing, the visibility data in the two IF channels were combined together and maps (generally of 512×512 pixels) made using the task ‘MX’. The visibility phases were then self-calibrated using one or two iterations of the task ‘SELFCAL’ before making the final maps.

The final maps generally had an rms noise level of 0.1 to 0.2 mJy per beam at 6 cm λ in most cases. The dynamic range achieved in these maps (defined as the ratio of the peak intensity to the rms value) was generally in the range of ~ 200 to 1500.

The maps of all the 45 sources are presented in Fig. 1 and some observed parameters are summarised in Table 1, which is arranged as follows:

Column 1: Source name in the IAU designation.

Column 2: An alternative name from a radio survey.

Column 3: Redshift (taken from Veron & Veron 1989 or Hewitt & Burbidge 1993).

Column 4: The total flux density at 4.86 GHz. For sources mapped also at 21 cm λ , the total flux density at 1.5GHz is listed on the second line in this column. In the case of large sources ($\text{LAS} \gtrsim 30 \text{arcsec}$) some extended flux may have been missed in the synthesis mapping for lack of short spacings, particularly at 6 cm λ . Flux density values for such sources are enclosed in parentheses.

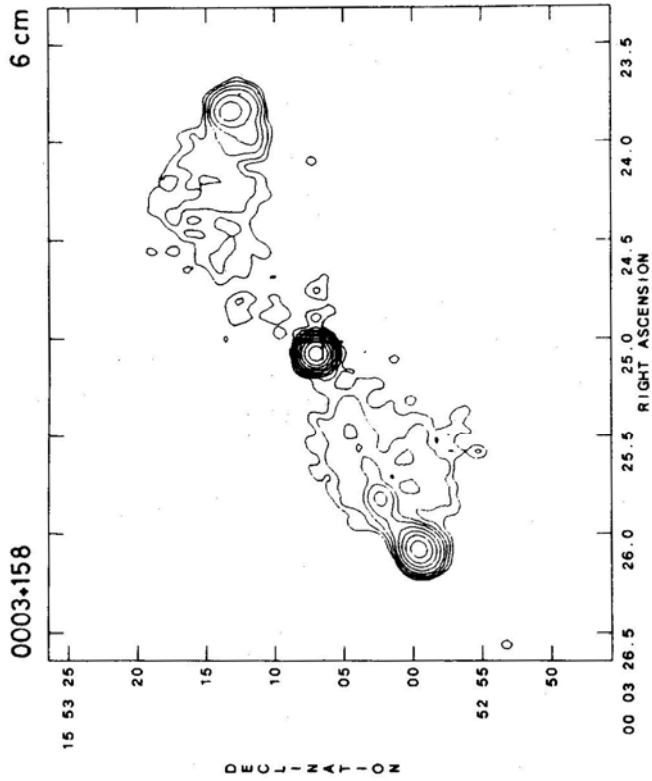
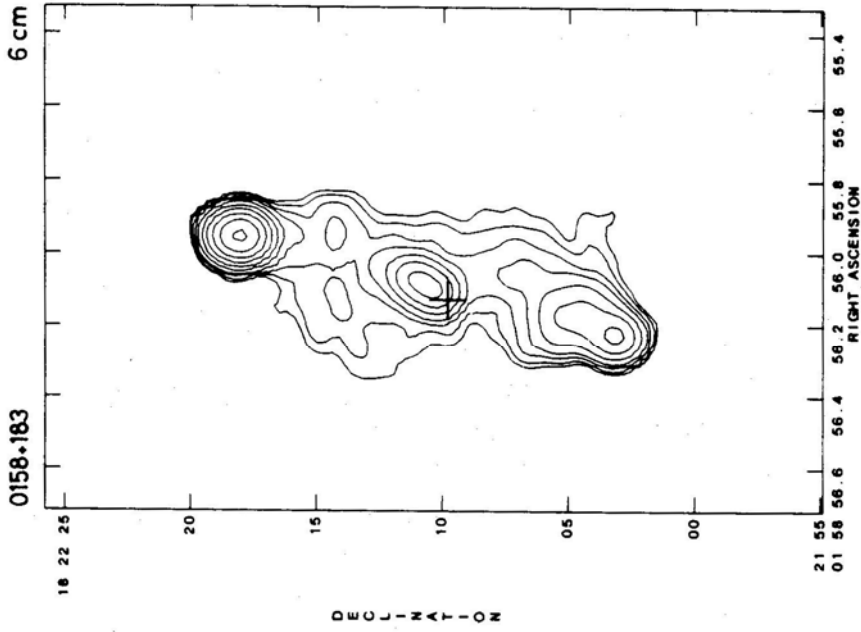


Figure 1. Contour plots of the radio images of 45 quasars. Optical positions of the quasars are indicated by the '+' signs. Negative contours are shown by dotted lines. The contours of total intensity are plotted at $C \times [-1, 1, 1.5, 2.5, 4, 8, 16, 32, 64, 128, \dots]$ mJy per beam area. The values of 'C' and the details about the gaussian restoring beams used in the plots are listed in Table 2.

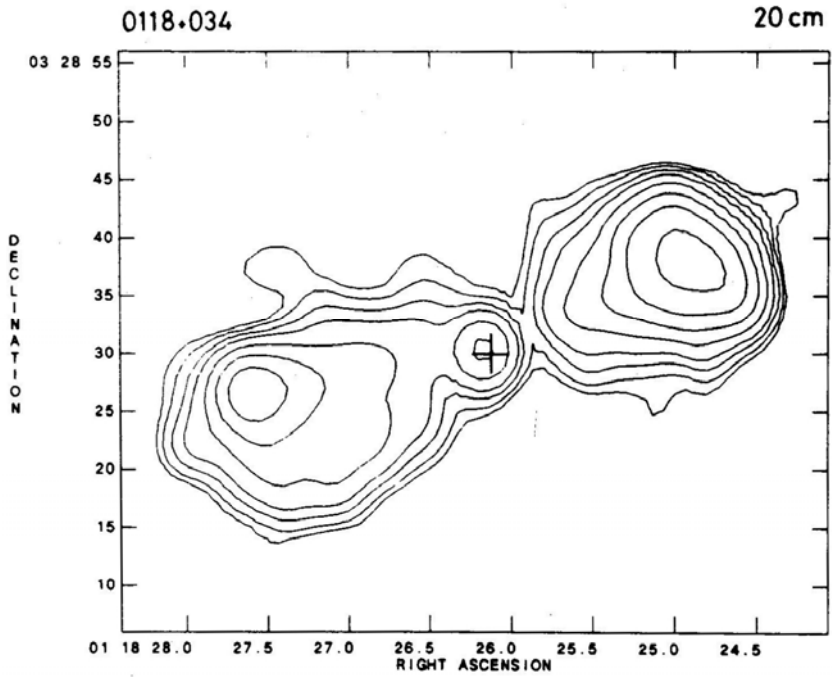
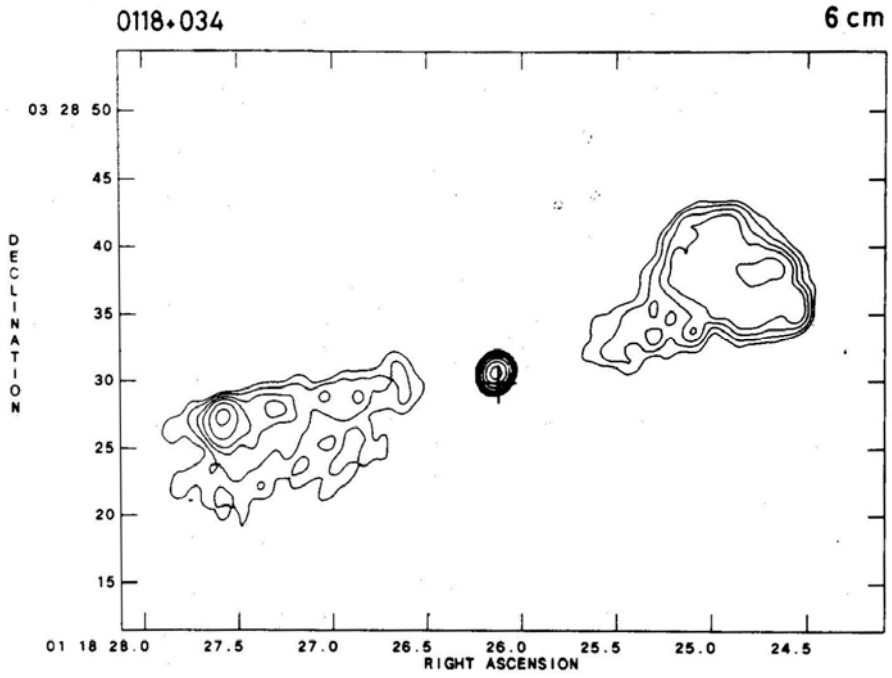


Figure 1(b).

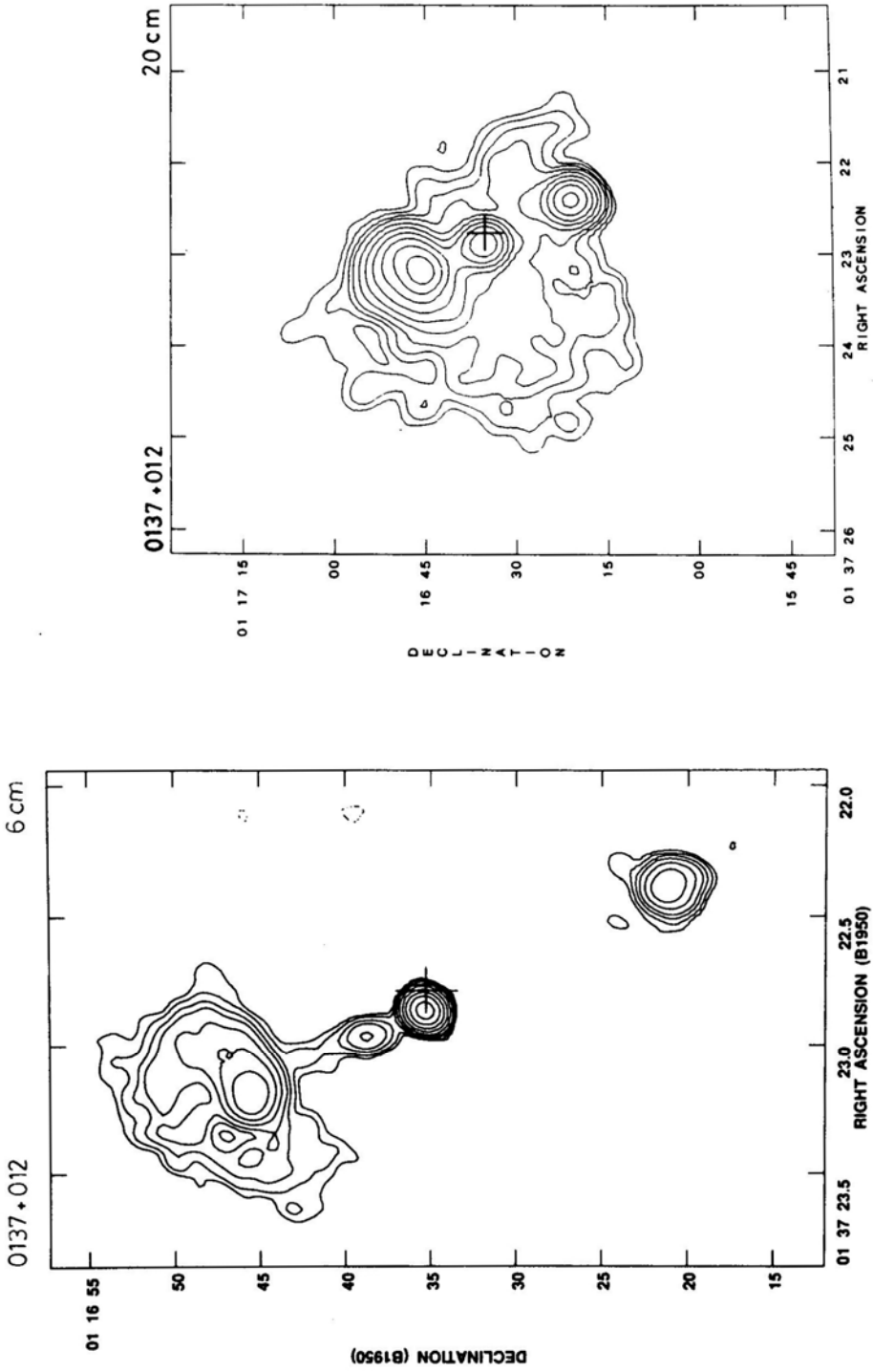


Figure 1(c).

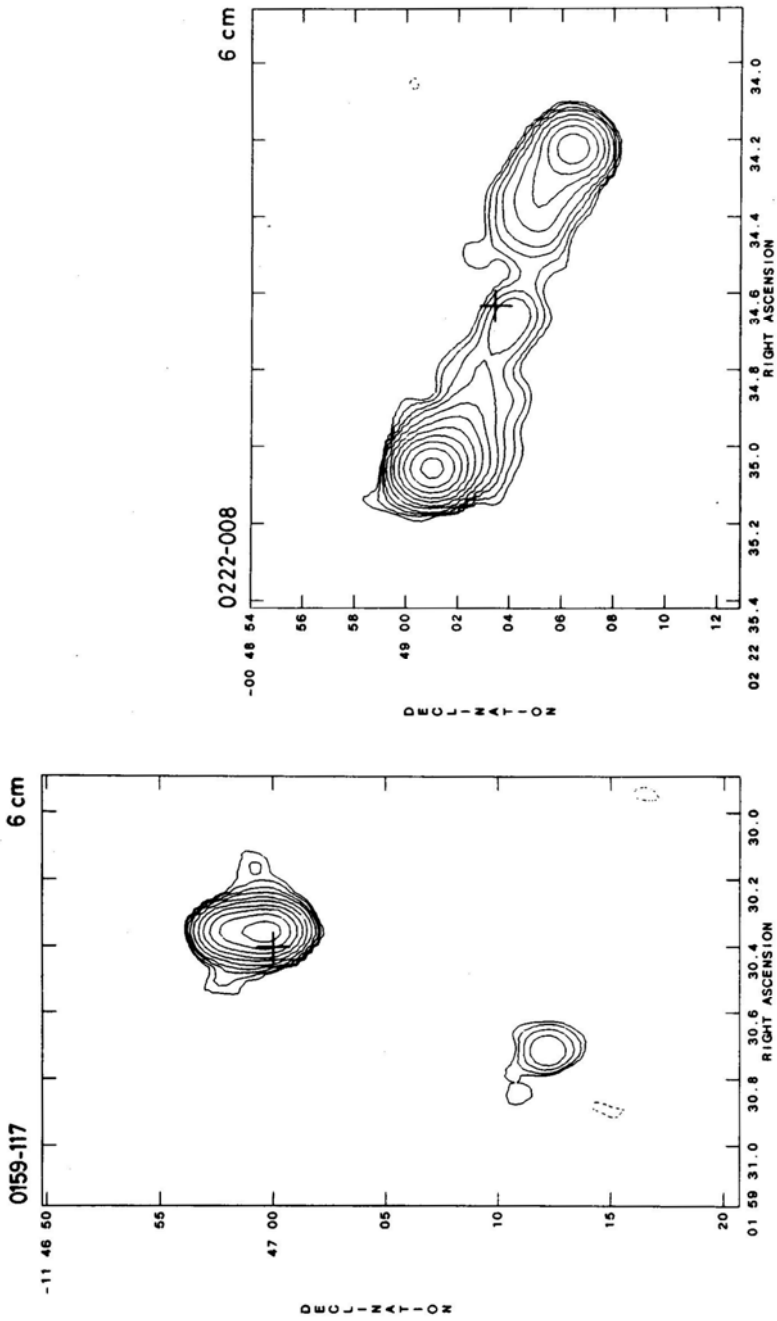


Figure 1(d).

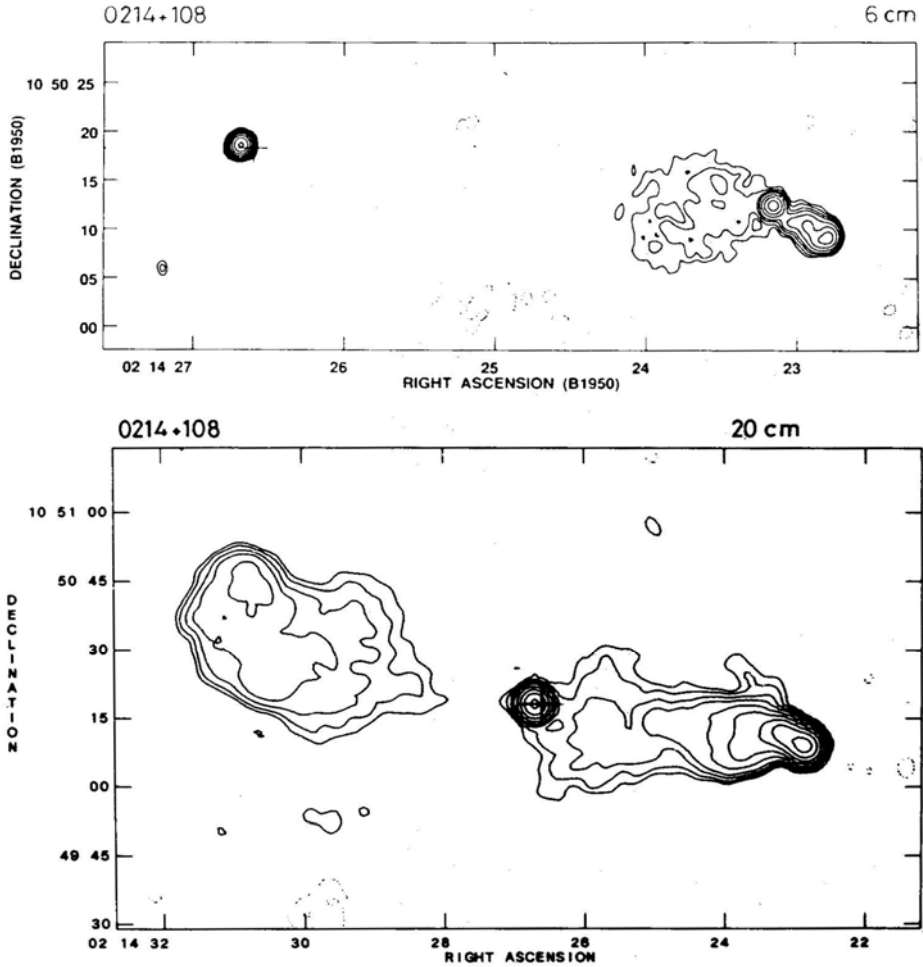


Figure 1(e).

Column 5: Flux density of the radio core component S_{core} at 4.84 GHz. The corresponding value at 1.5 GHz is listed on the second line in some cases.

Columns 6 & 7: The right ascension and declination (1950.0) of the radio core component. The accuracy in the position should generally be better than ± 0.5 arcsec.

Columns 8-10: The optical position of the quasar. Only the seconds of right ascension and arcseconds of the declination are listed in columns 8 and 9 respectively. The reference to the optical position is coded in column 10. The positions are generally accurate to better than ± 1 arcsec.

Column 11: The largest angular size (LAS) in seconds of arc. LAS is defined as the separation between the hotspots or the brightest features in the two lobes.

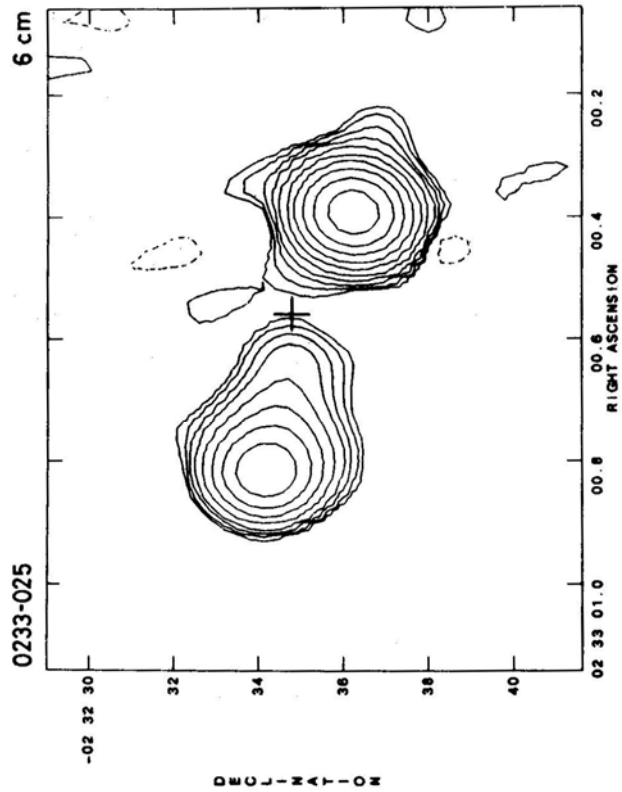
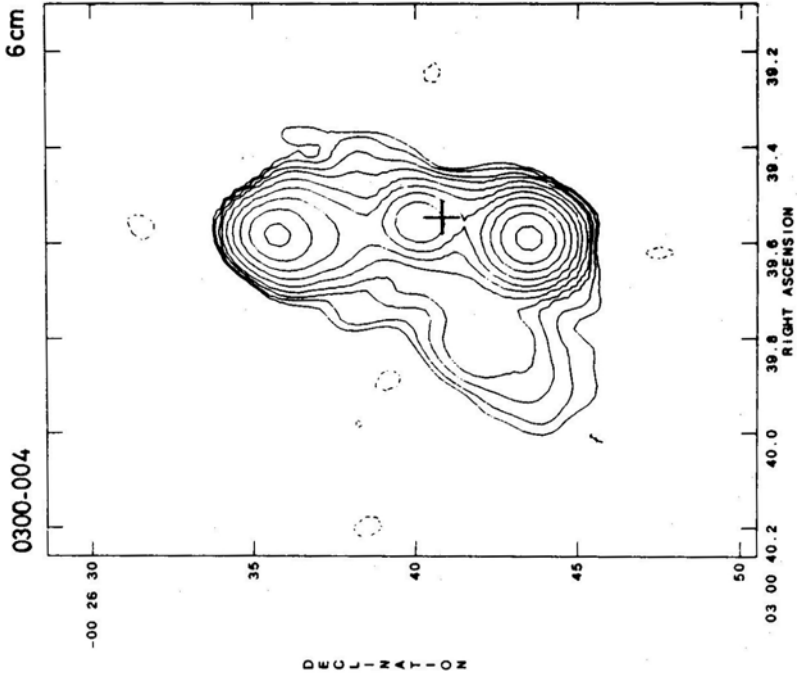


Figure 1(f).

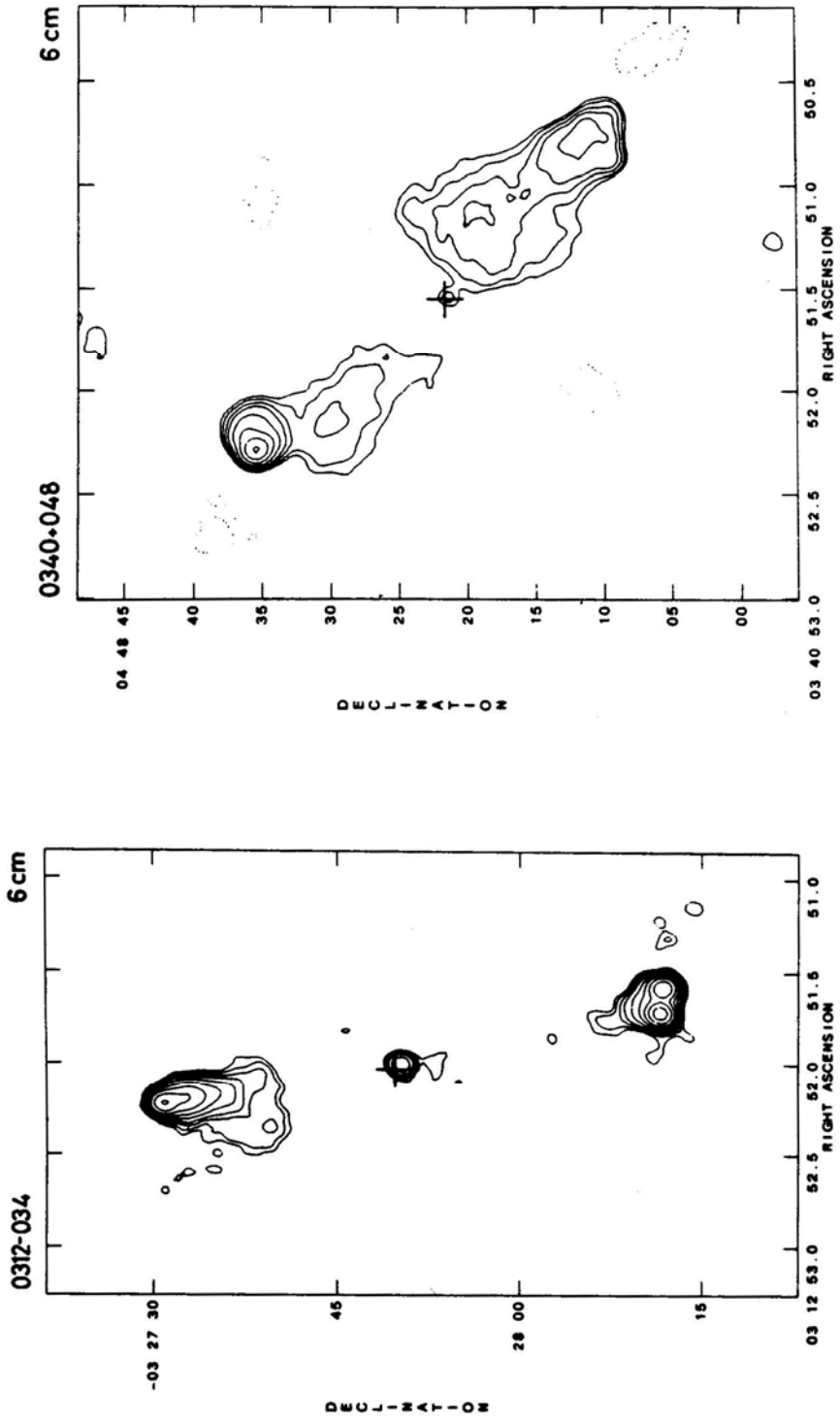


Figure 1 (g).

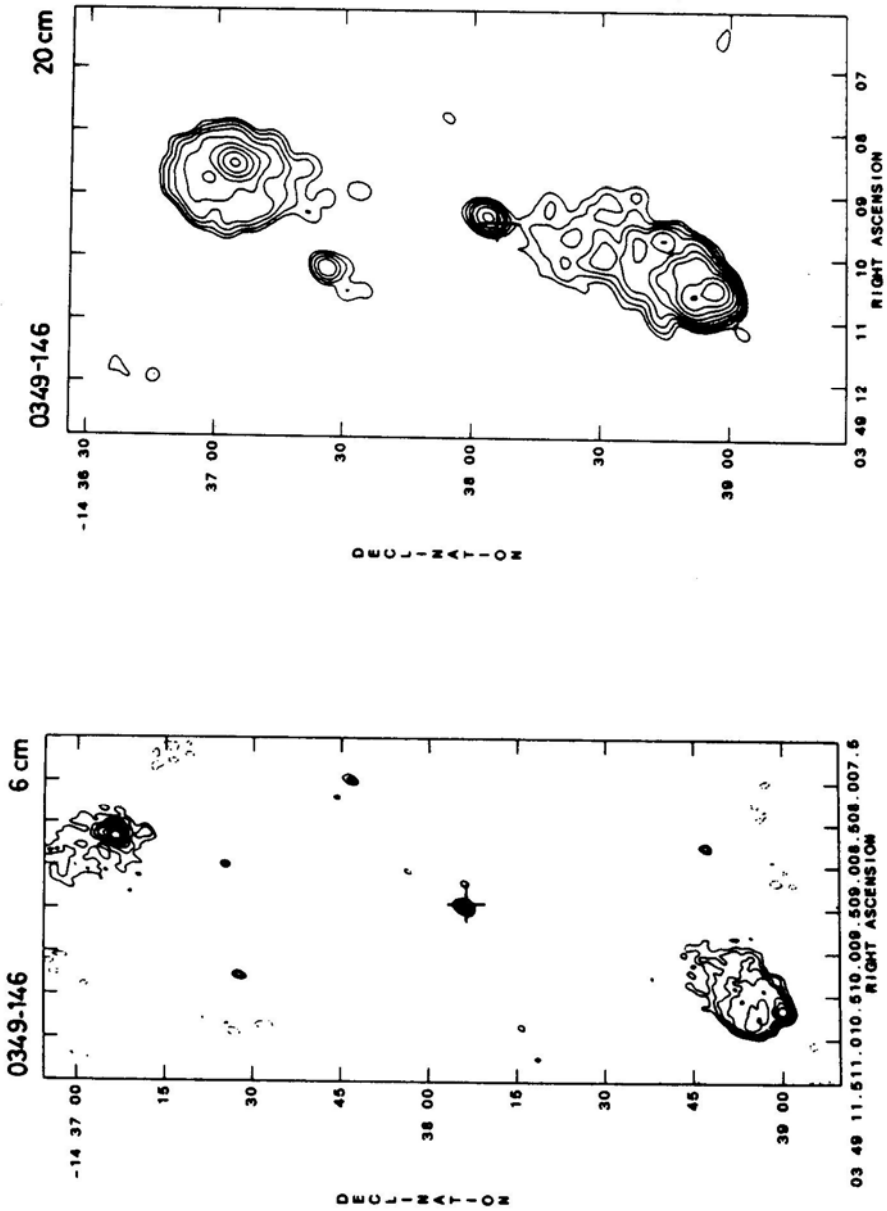


Figure 1(h).

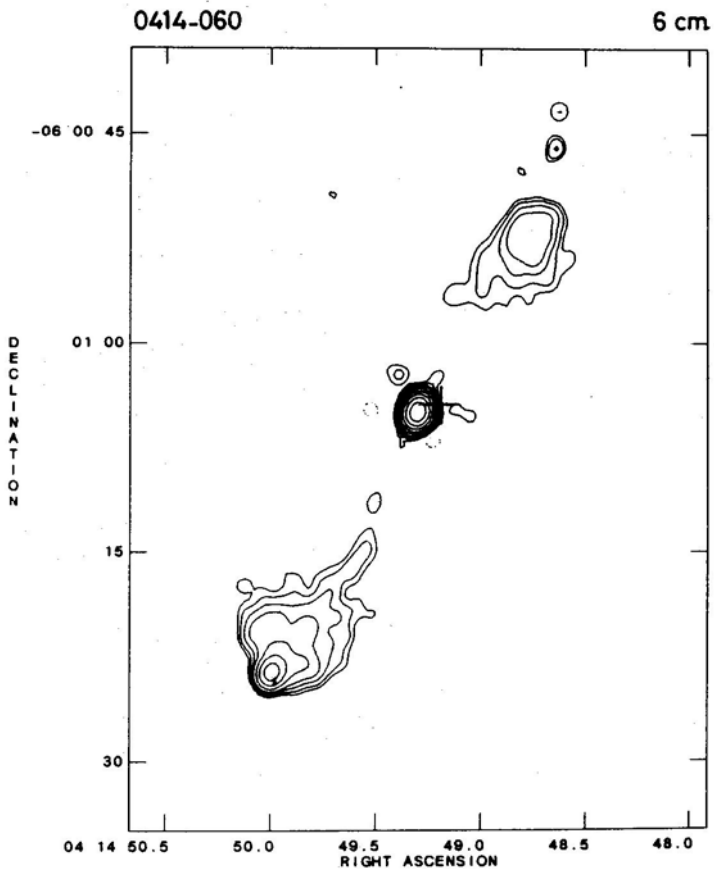
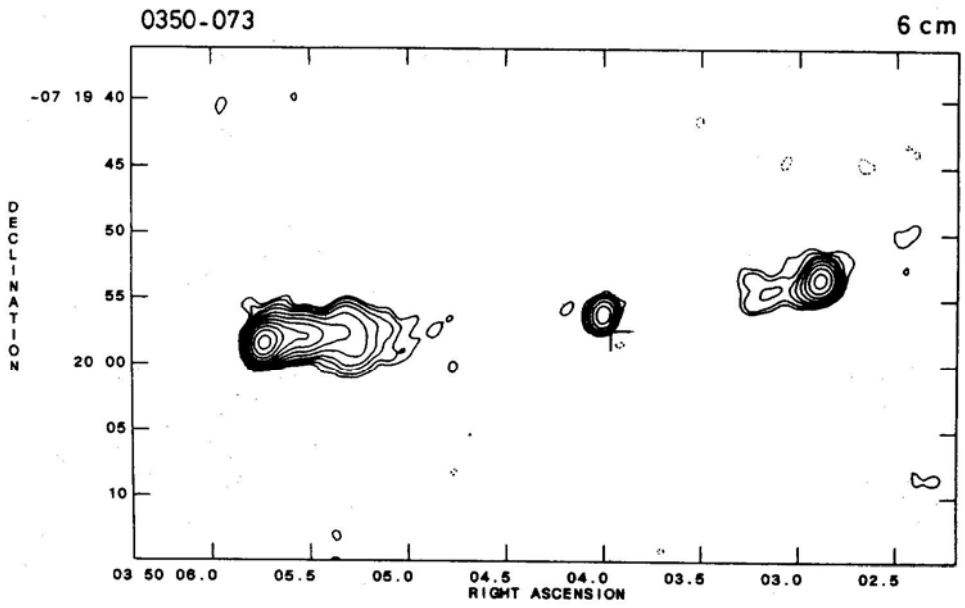


Figure 1(i).

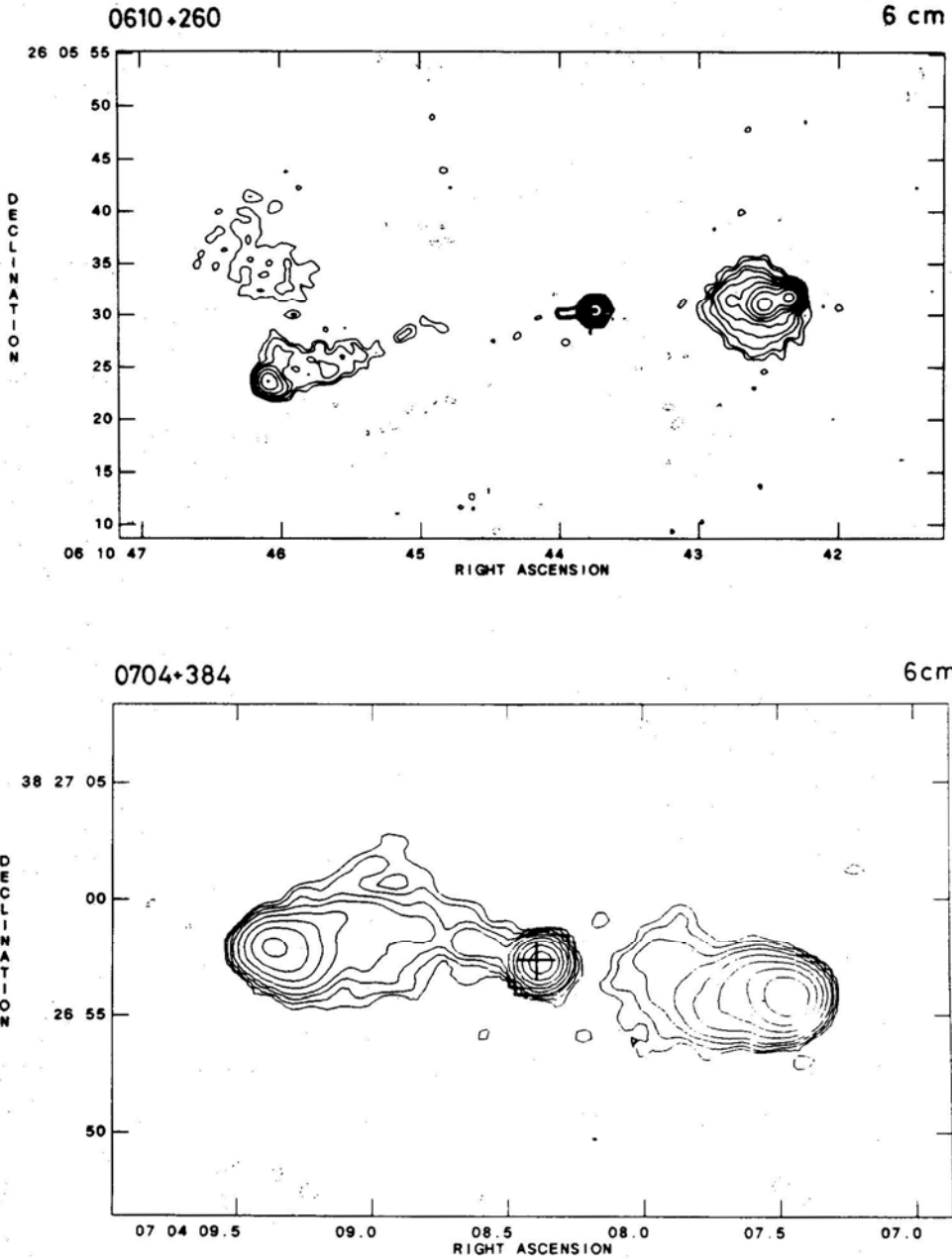


Figure 1(j).

Asterisks in the table refer to additional notes in the text on some objects at the end of this section.

Information on the contour values and the restoring beams used in the maps shown in Fig. 1 is summarised in Table 2. While the typical rms noise in each map is listed in column 2, the peak value of the flux density, in mJy is given in column 3 and the value of

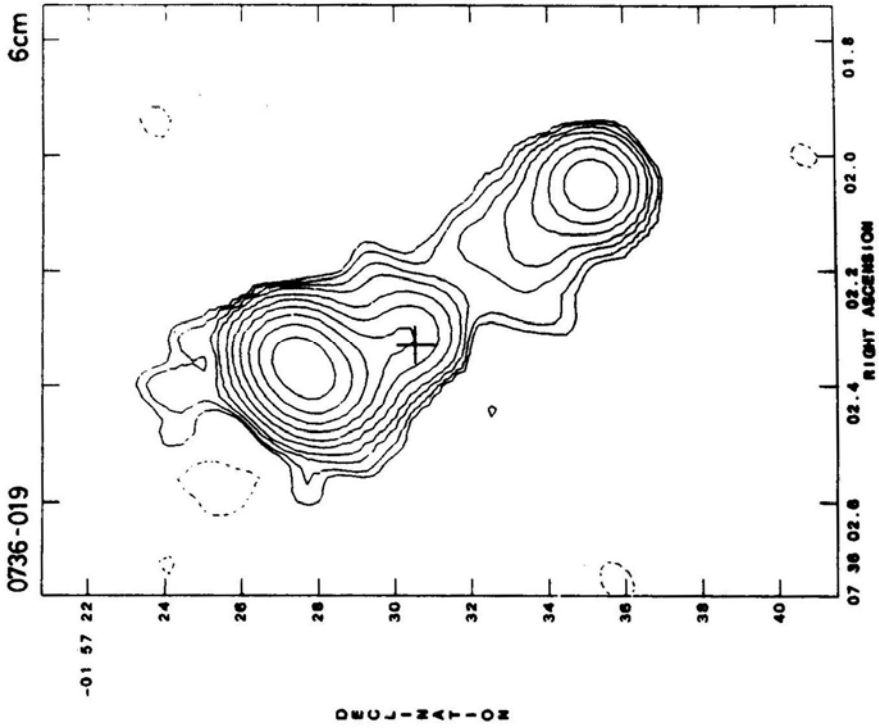
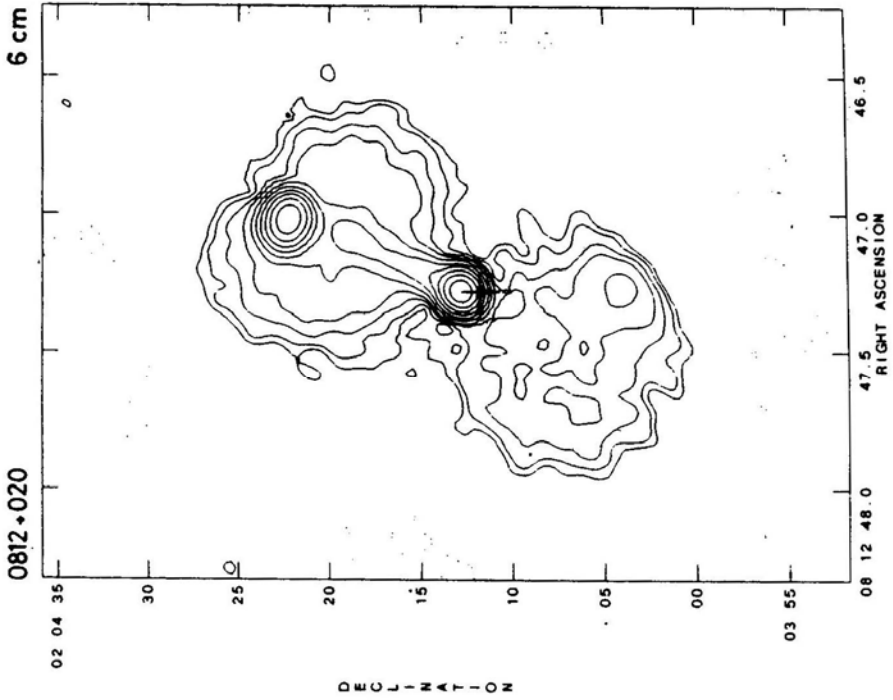


Figure 1 (k).

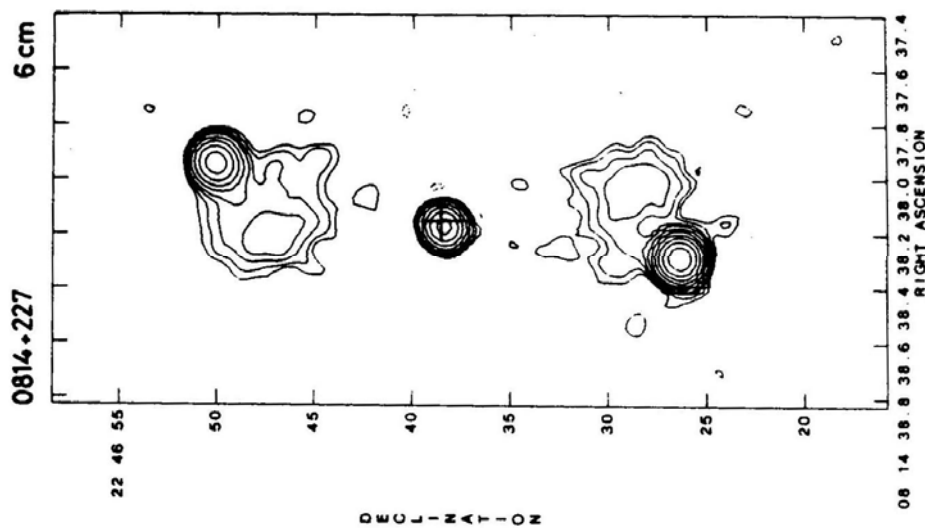
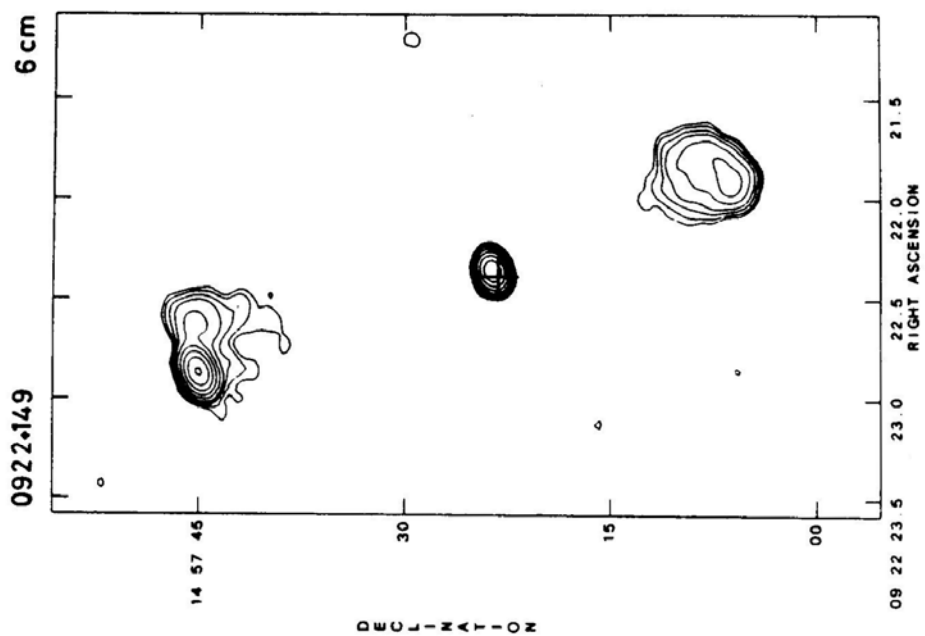


Figure 1(l).

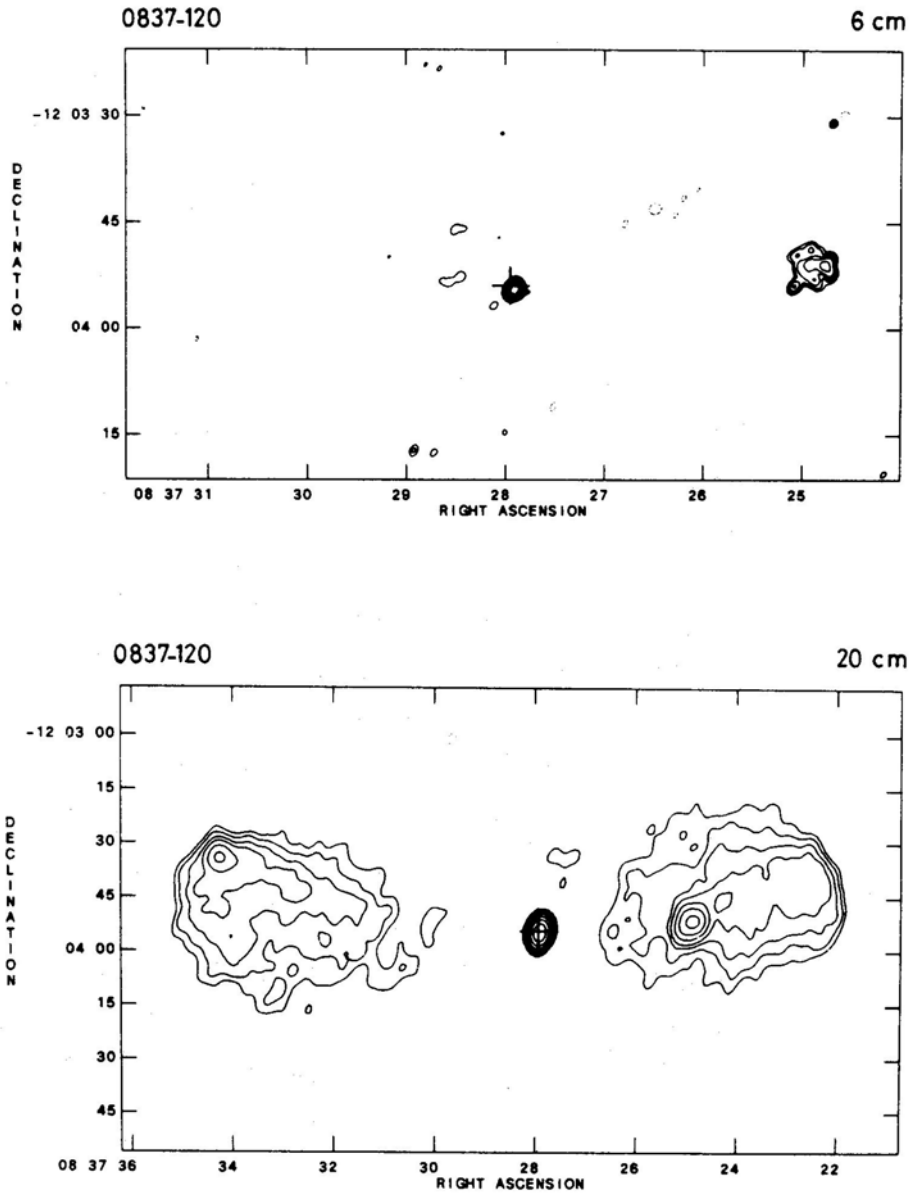


Figure 1(m).

the first positive contour (C), in mJy per beam area, is given in column 4. The contours plotted in the corresponding maps in Fig. 1 are at $C \times (-1, 1, 1.5, 2.5, 4, 8, 16, 32, 64, 128 \dots)$ mJy/beam area.

The half power widths of the major and minor axes of the restoring Gaussian beam widths and the position angles of the major axes are listed in columns 5, 6 and

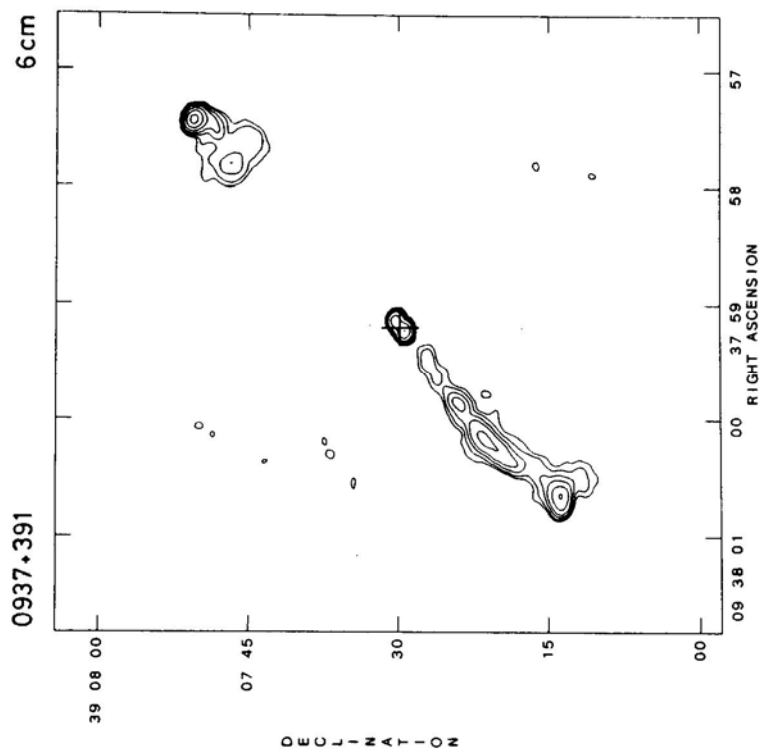
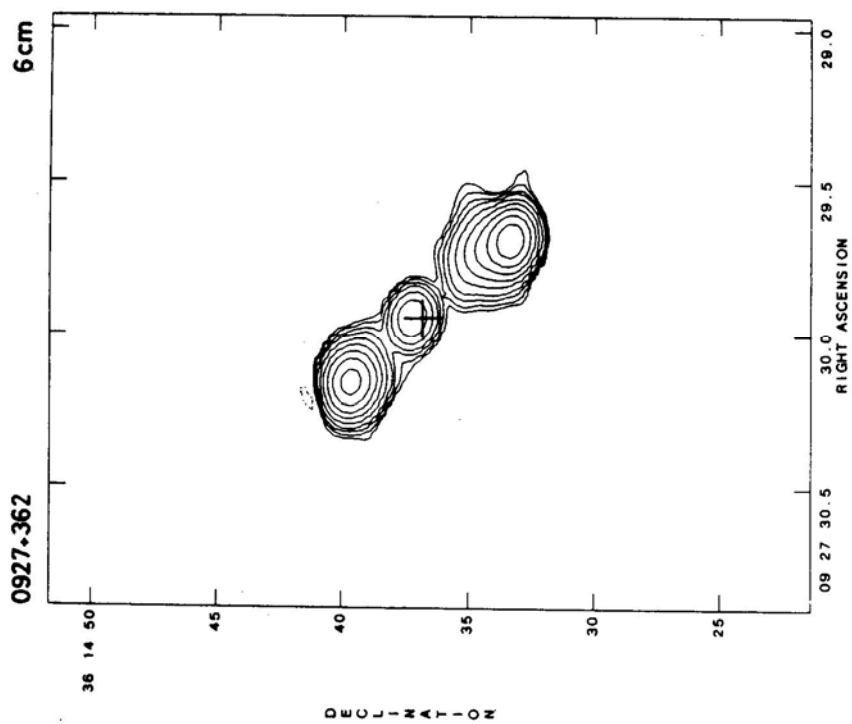


Figure 1 (n).

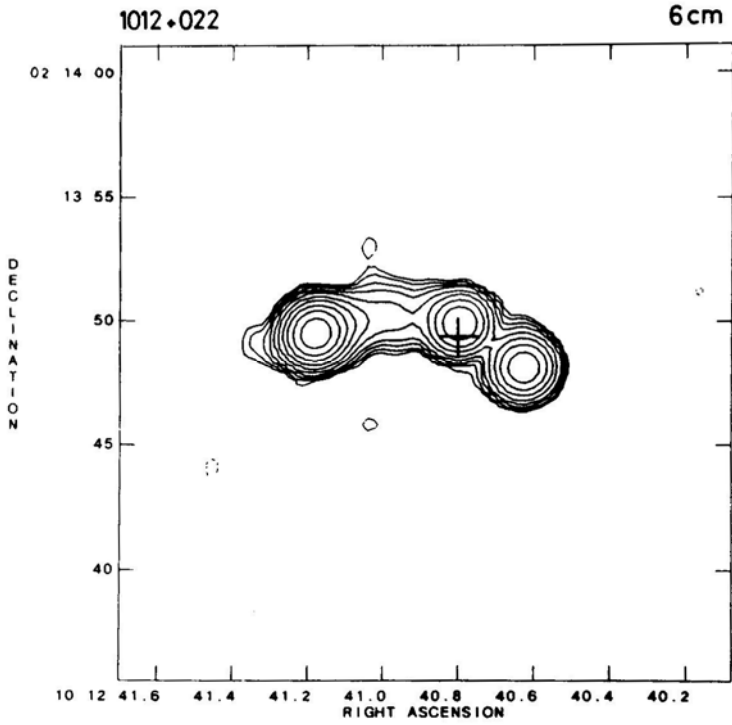
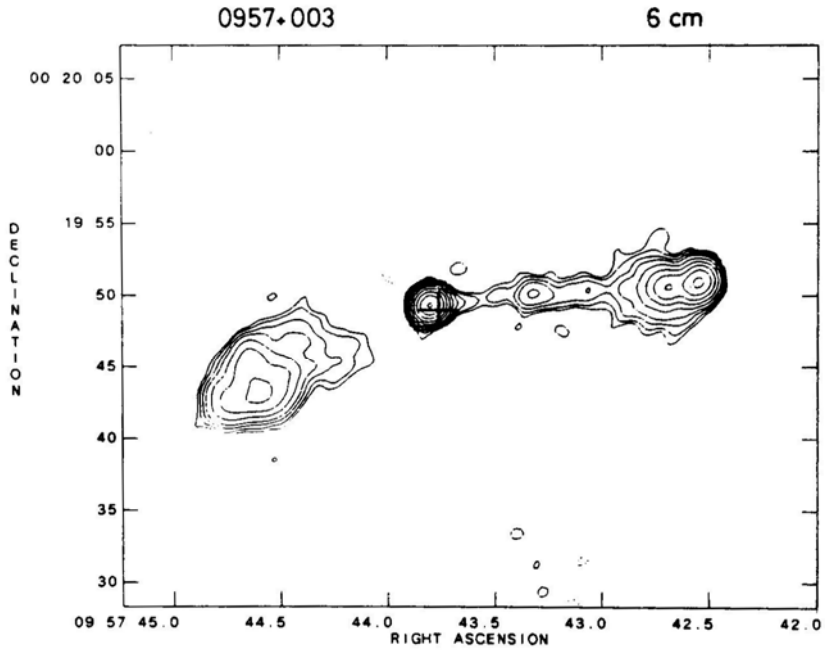


Figure 1(o).

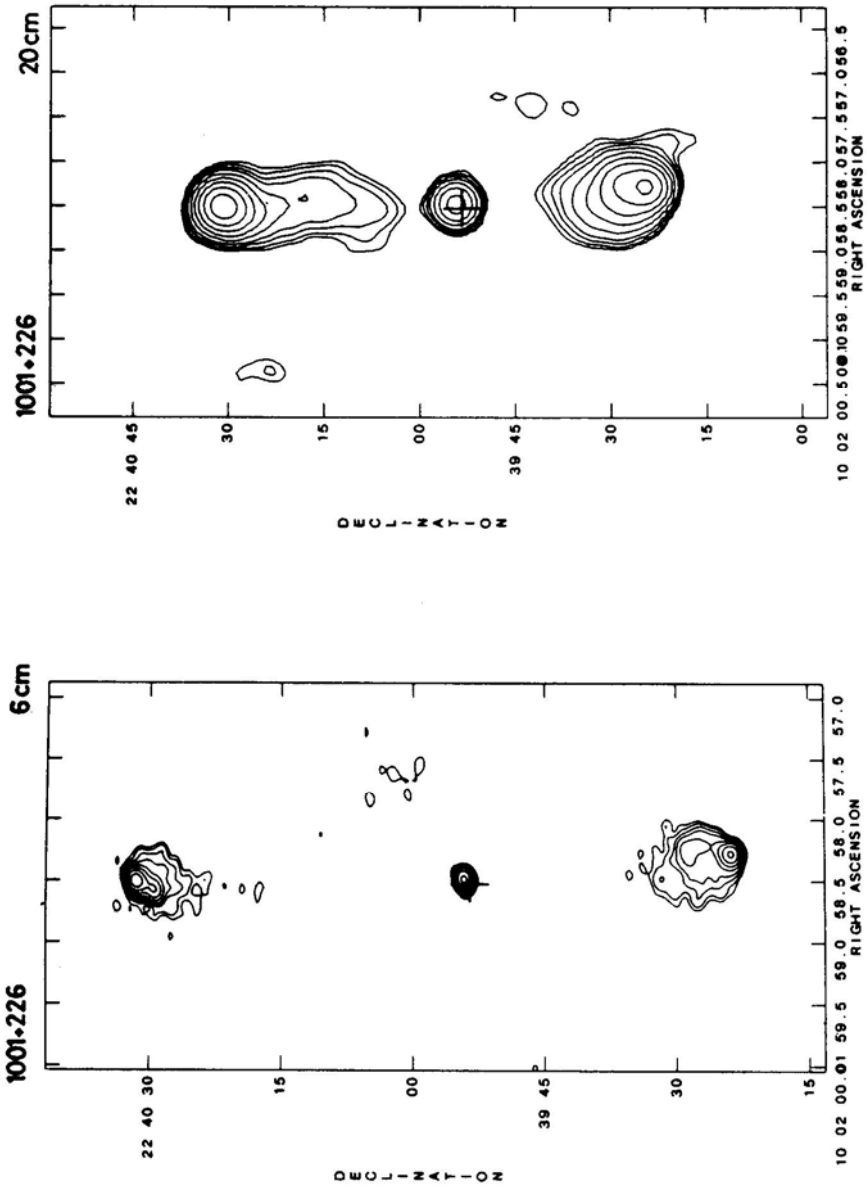


Figure 1 (p).

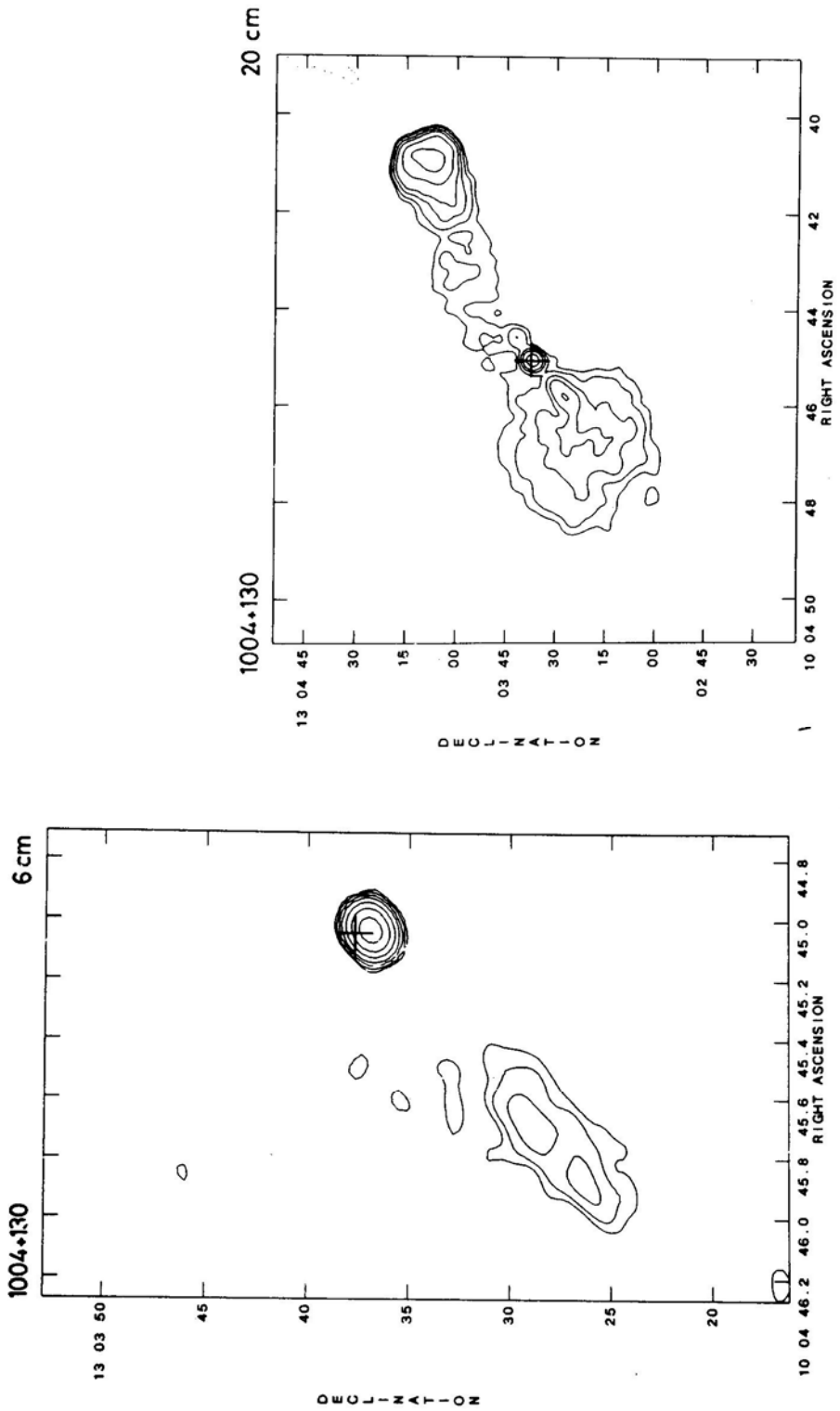


Figure 1(q).

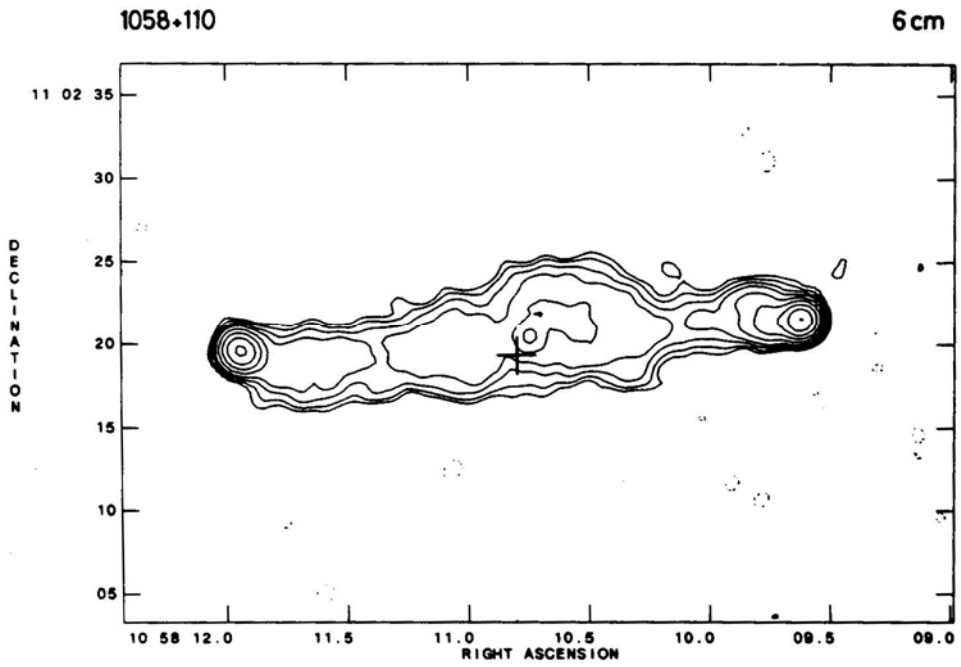
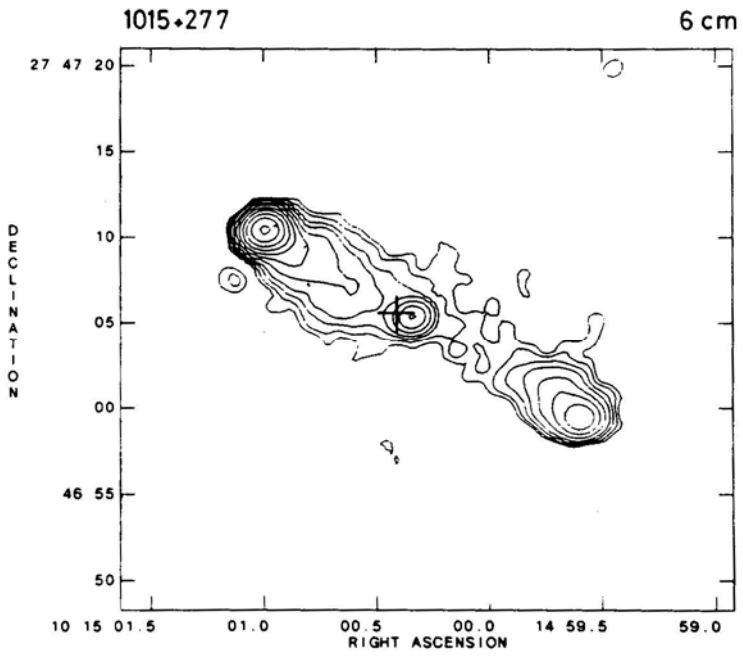


Figure 1(r).

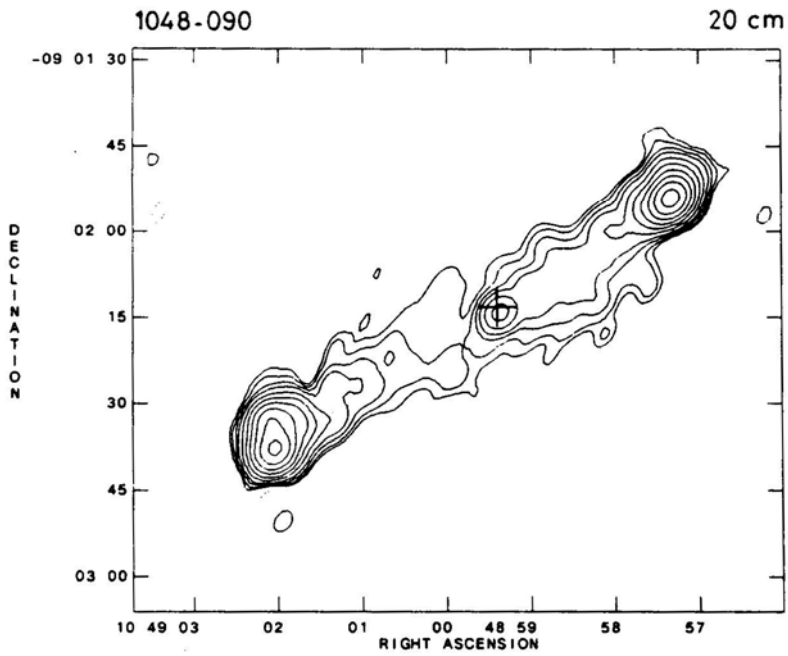
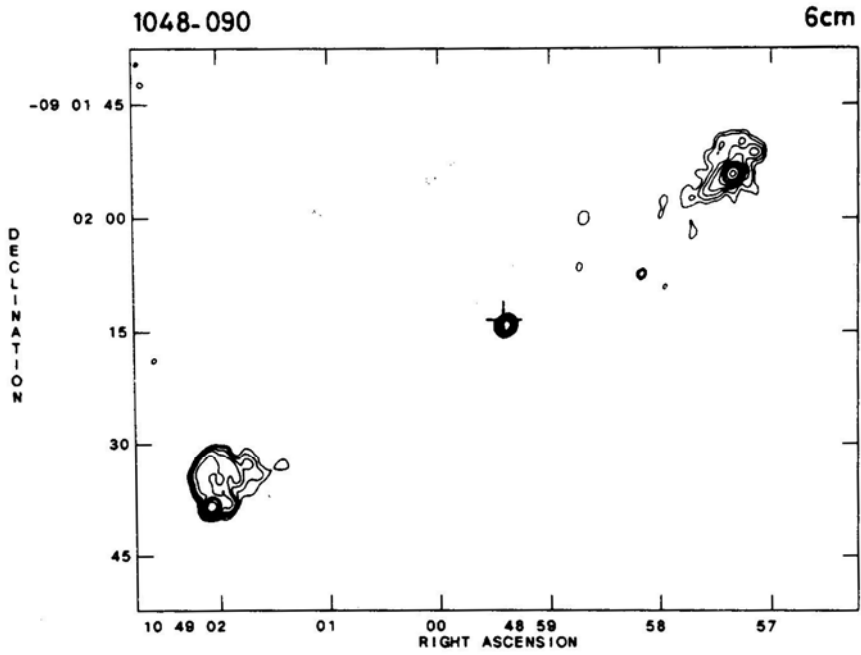


Figure 1(s).

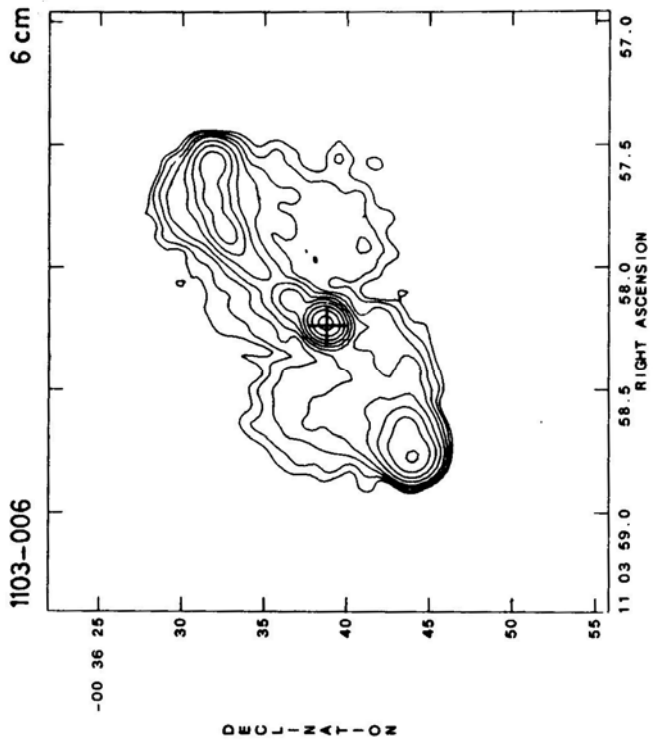
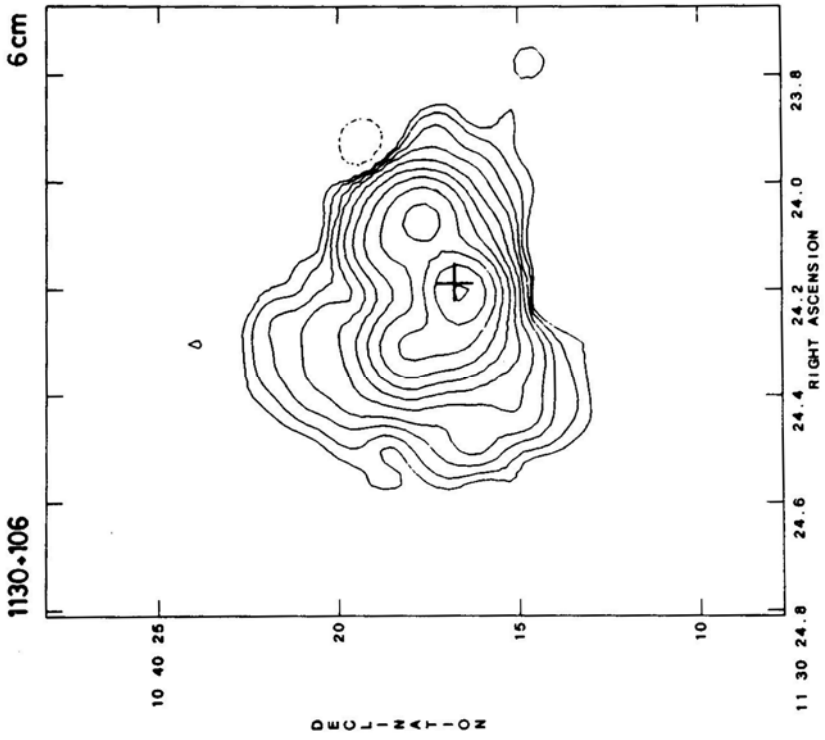


Figure 1(t).

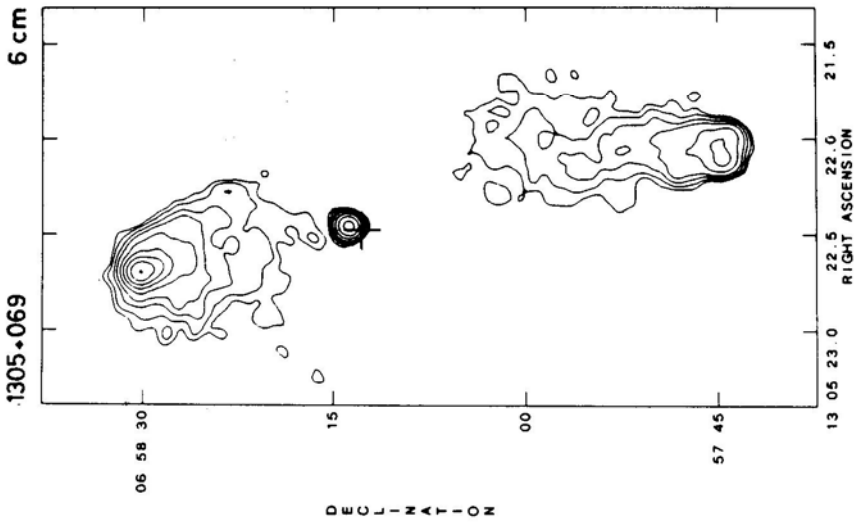
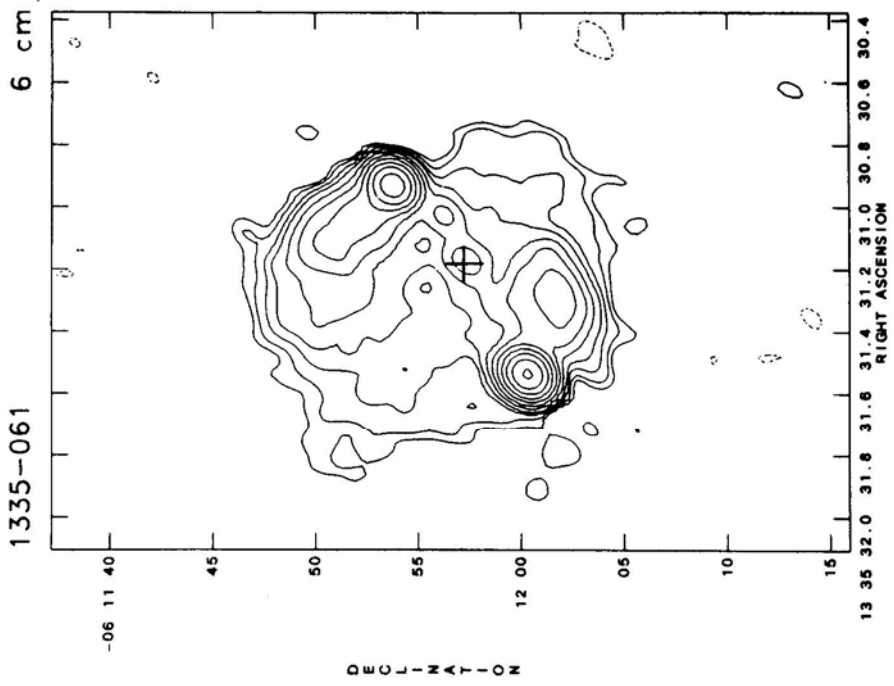


Figure 1(u).

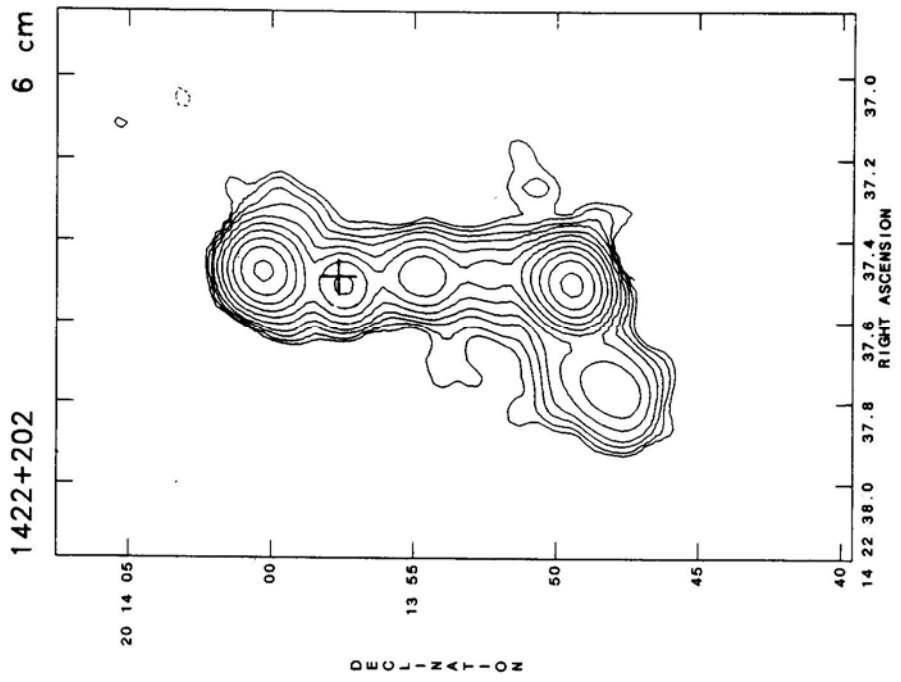
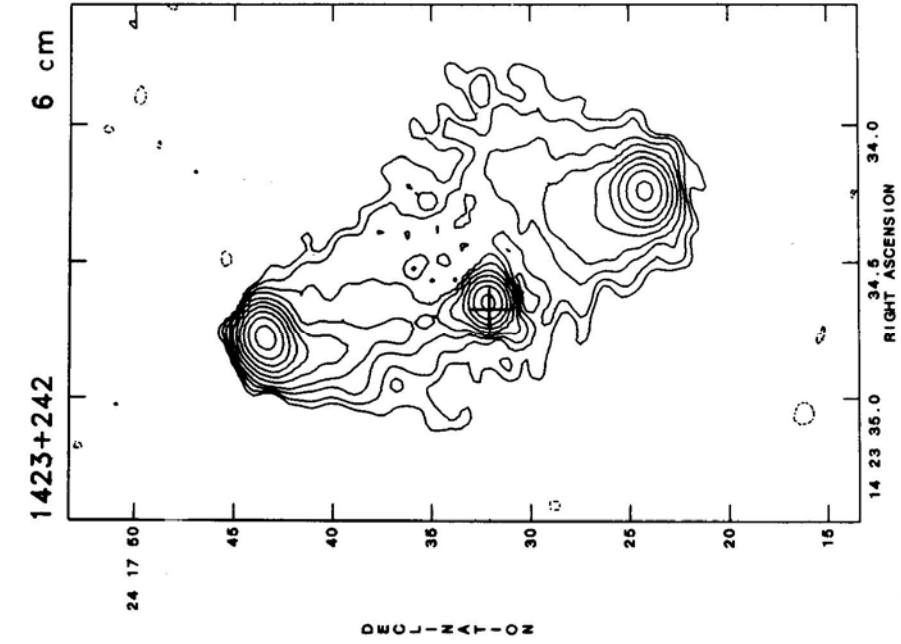


Figure 1(v).

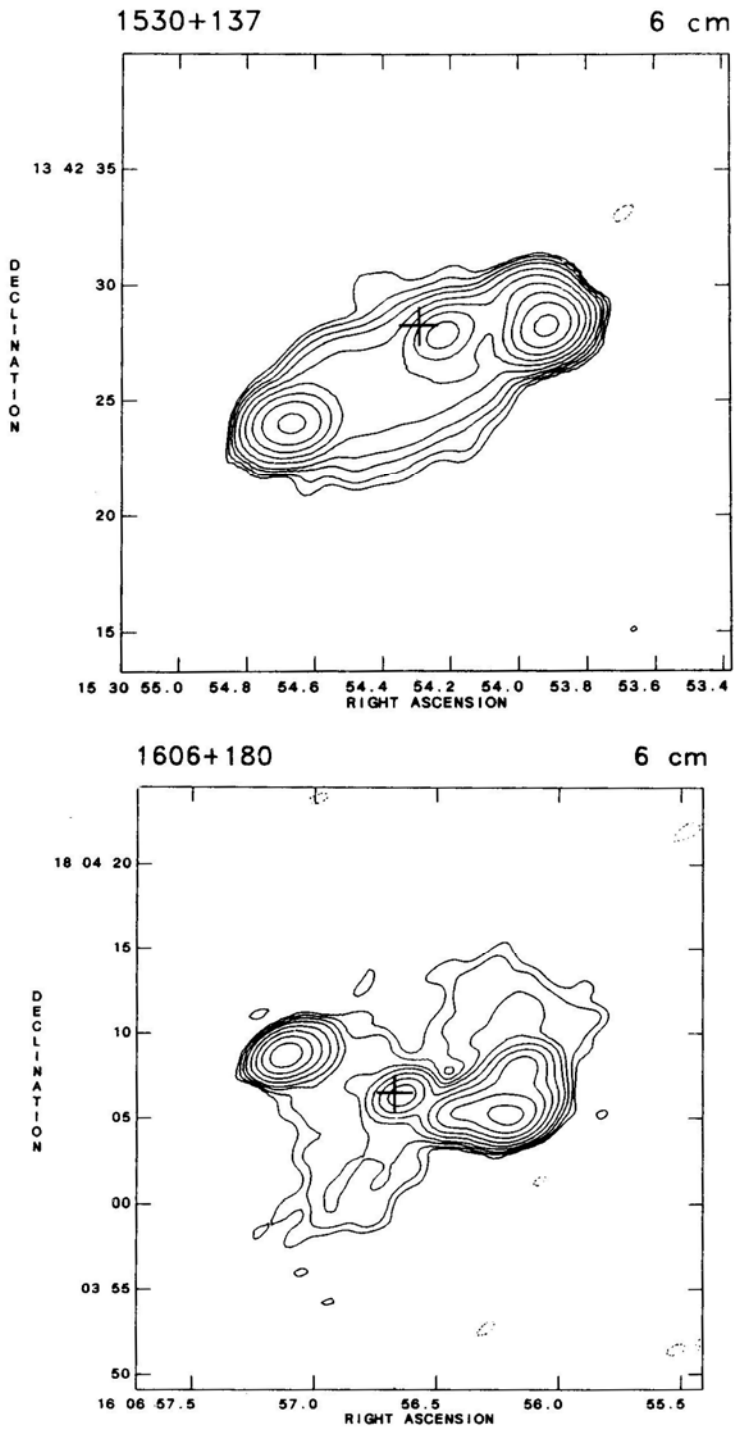


Figure 1(w).

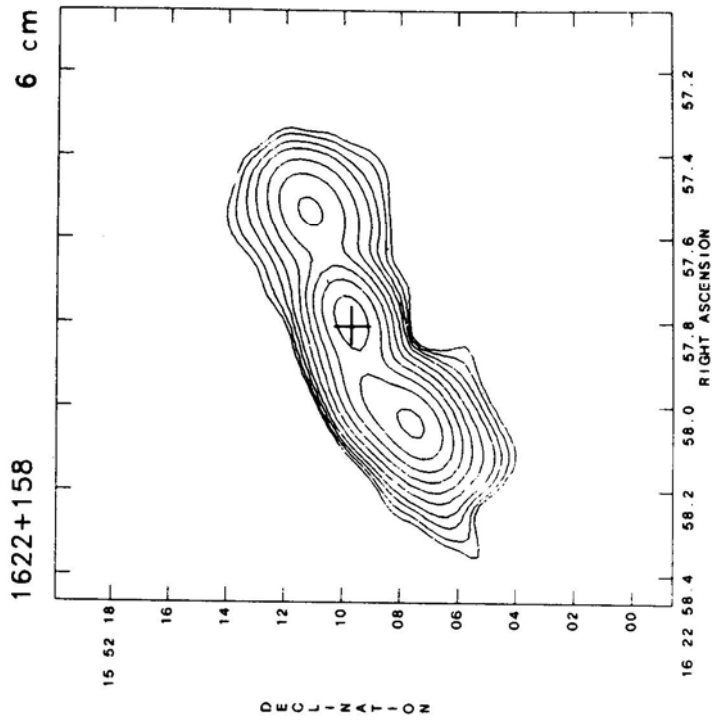
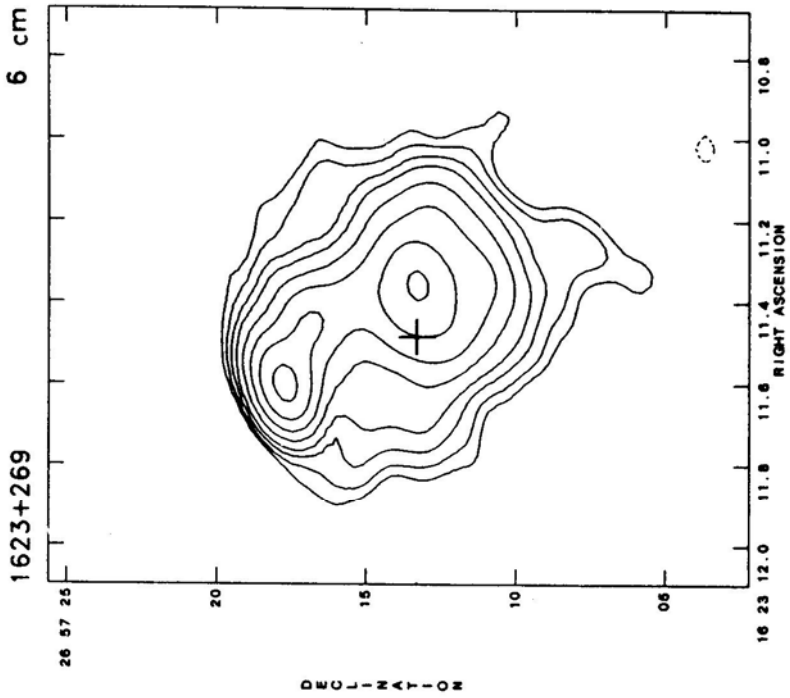


Figure 1(x).

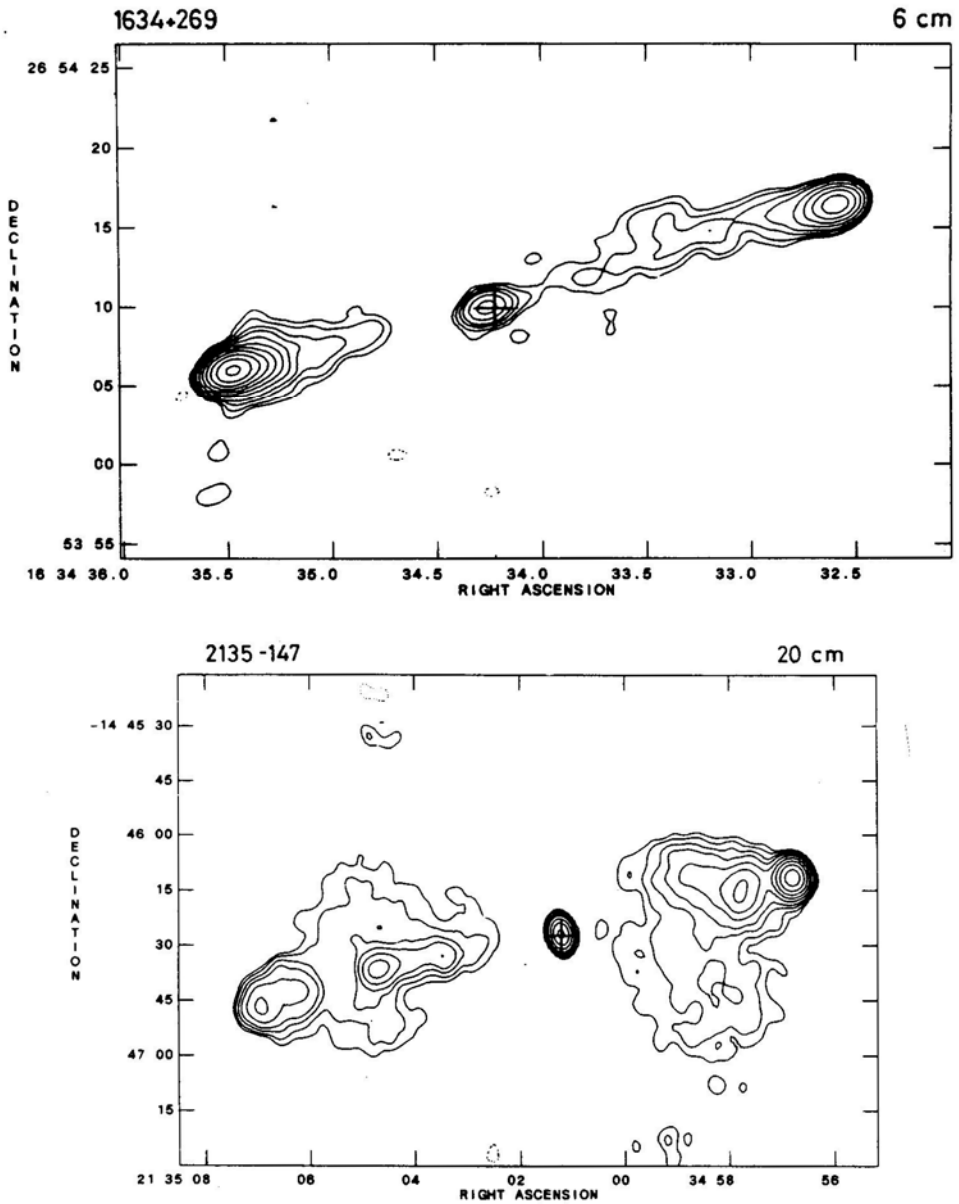


Figure 1(y).

7 respectively. As in Table 1, entries on the second line for any source refer to the source maps at 20 cm λ .

Notes on some individual sources

0137 + 012: Our 20 cm map shows considerably more extended emission surrounding the two lobes than seen in the earlier 20 cm map by Hintzen *et al.* (1983).

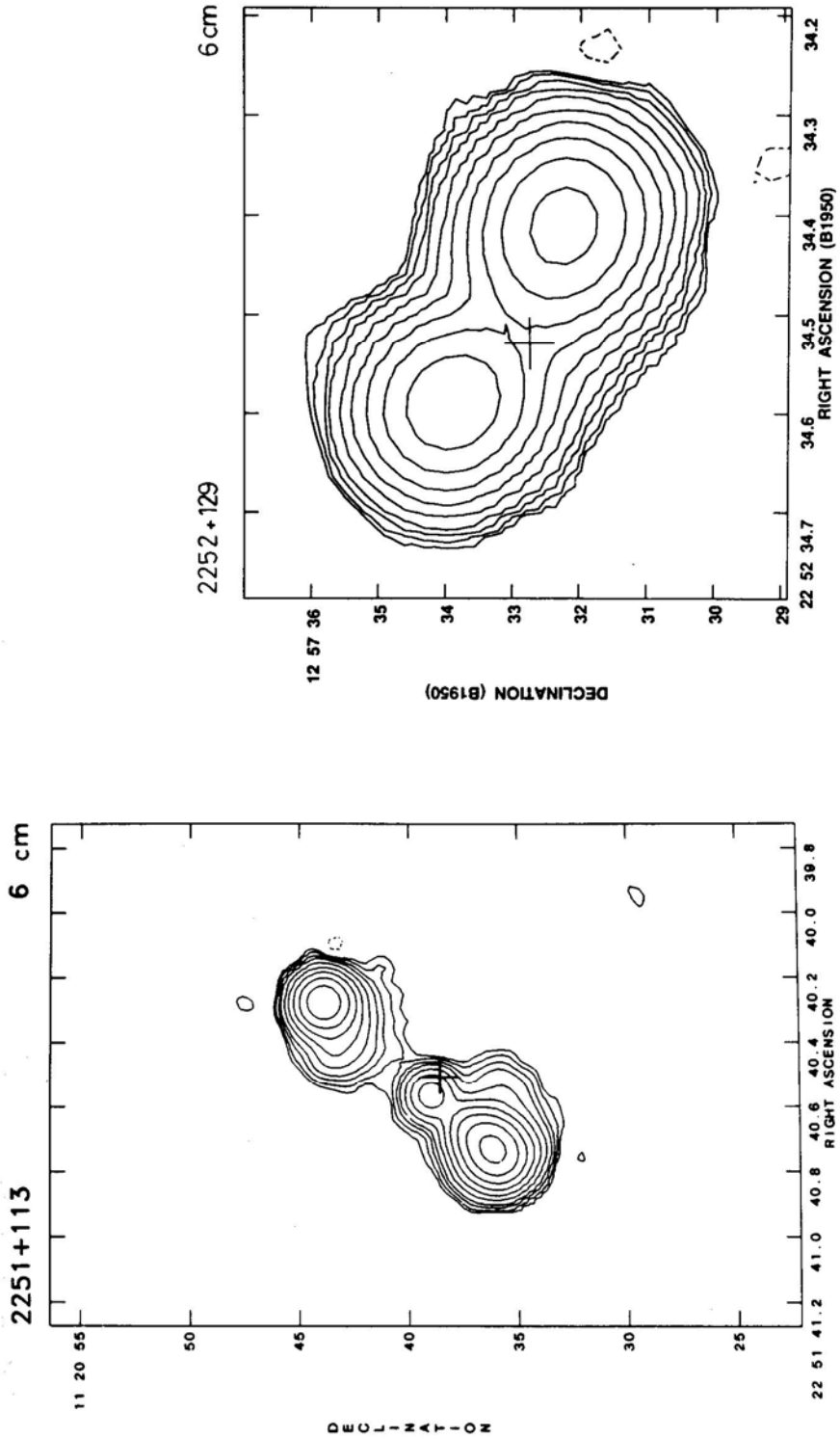


Figure 1(z).

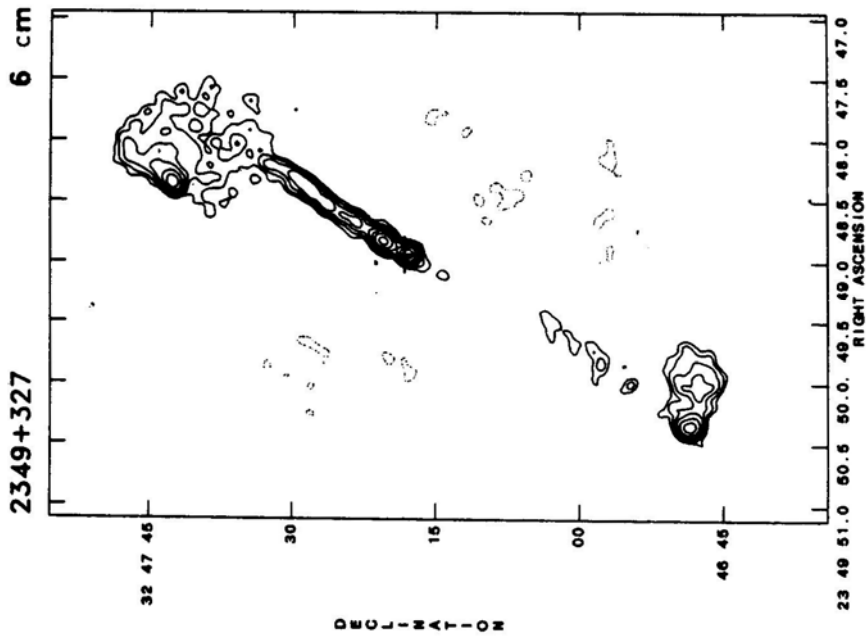
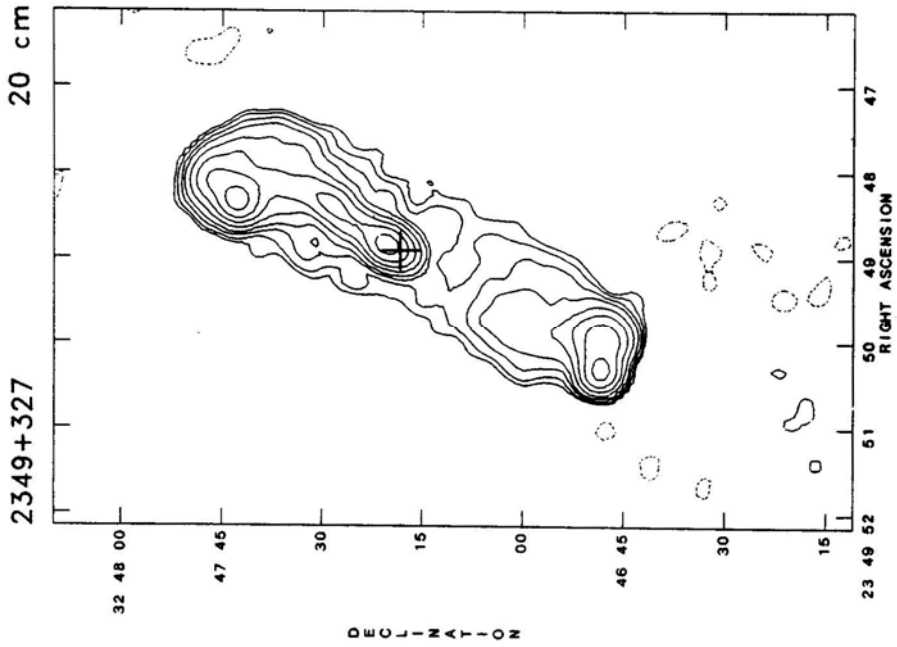


Figure 1(A).

- 0158 + 183:** The core flux of 40 mJy includes a contribution from part of a nuclear jet.
- 0159 – 117:** The weak component, 13.7arcsec SE of the optical quasar has a flux density of $S_{6\text{cm}} = 20$ mJy. It was not seen in the earlier 20 cm map of Hintzen *et al.* (1983). The radio structure thus appears to be quite asymmetric. The other lobe which is much stronger, appears to lie only about 1.5 arcsec north of the core and is not fully resolved with the present resolution. In a higher resolution map at 6 cm λ , published recently by Price *et al.* (1993), the northern component is clearly separated from the core and faint emission is seen also from the weaker SE lobe.
- 0214 + 108:** The eastern lobe is totally resolved out in the 6 cm observations.
- 0233 – 025:** This is one of the very few quasars in the sample in which a radio core component was not detected.
- 0300 – 004:** There is considerable amount of off axis extended emission to the east and northeast of the southern hotspot.
- 0610 + 260:** The eastern lobe has extended emission almost at right angles to the source axis.
- 0736 – 019:** This source was earlier classified to be of D2 type radio structure by Hintzen *et al.* (1983), possibly because of an incorrect optical position of the quasar plotted on their VLA map. The present map shows a triple structure with the optical position of McEwan *et al.* (1975) close to a possible radio core.
- 0812 + 020:** Hintzen *et al.* (1983) considered this source to have D2 type structure as the extended southeastern lobe was not seen in their 20 cm VLA map. This lobe is resolved out also in the higher resolution 6 cm map of Price *et al.* (1993).
- 0814 + 227:** Both the lobes appear to be extended at large angles to and on opposite sides of the axis defined by the hotspots.
- 0837 – 120:** The eastern lobe clearly seen in the 20 cm map has been resolved out in our 6 cm map.
- 0937 + 391:** It is difficult to identify the radio core as there are two compact components close to the optical position. The total flux density of the two components at 6cm λ is 14 mJy. We have considered the northwest component to be the radio core because it is found to have a flatter spectral index between 20 cm and 6 cm as noted by Price *et al.* (1993). The southern lobe thus appears to consist of a long jet with several knots in it.
- 0957 + 003:** The jet connecting the core to the western lobe, seen in our map is resolved out in the higher resolution map of Price *et al.* (1993).
- 1004 +130:** Most of the extended structure in the lobes seen in our 20 cm map is resolved out at 6 cm λ .
- 1012 + 022:** The lobes are strongly non collinear with respect to the radio core.
- 1130 +106:** The higher resolution 6 cm map of Price *et al.* (1993) confirms that the radio peak close to the optical position is indeed the radio core. The lobes are thus strongly misaligned with the core.
- 1335 – 061:** The two lobes have emission extended at large angles to the axis defined by the hotspots.
- 1422 + 202:** There appears to be a sharp bend in the radio structure near the southern end.

Table 1. Radio structure of 45 quasars.

Source	Other name	Redshift	S_{total} (mJy)	S_{core} (mJy)	h	m	s	Radio Core Posn. (1950.0)	Opt. posn. s	Opt. posn. "	Ref. pos.	LAS (" arc)
0003 + 158	4C15.01	0.45	315	109	00	03	25.07	15 53 07.0	25.01	06.6	1	35.1
0118 + 034	4C03.04	0.765	296	29	01	18	26.13	03 28 30.7	26.12	29.9	2	45.0
			945	37								
0137 + 012	4C01.04	0.260	515	150	01	37	22.86	01 16 35.3	22.78	35.2	1	27.5*
			1240	185								
0158 + 183	4C18.07	0.799	325	40*	01	58	56.09	18 22 10.7	56.13	09.8	3	15.0
0159 - 117	3C57	0.669	1195	*	01	59	30.36	-11 46 59.4*	30.40	00.0	4	15.5
0214 + 108	4C10.06	0.408	(297)	76	02	14	26.68	10 50 18.6	26.60	18.3	1	121.0*
			1163	82								
0222 - 008	PKS	0.687	405	5	02	22	34.68	-00 49 04.0	34.63	03.4	5	13.6
0233 - 025	PKS	1.322	315	*					00.56	34.8	1	6.5
0300 - 004	PKS	0.693	385	48	03	00	39.56	-00 26 40.1	39.55	40.9	6	7.8*
0312 - 034	PKS	1.072	335	7	03	12	52.00	-03 27 50.3	52.04	49.8	3	41.0
0340 + 048	3CR93	0.357	580	4	03	40	51.53	04 48 21.2	51.54	21.7	7	33.1
0349 - 146	3C95	0.614	(480)	46	03	49	09.47	-14 38 05.9	09.45	06.4	1	117.0
			2720	48								
0350 - 073	3C94	0.962	675	14	03	50	04.00	-07 19 56.1	03.97	57.4	1	42.1
0414 - 060	3C110	0.781	290	144	04	14	49.30	-06 01 04.9	49.18	04.3	8	36.4
0610 + 260	3CR154	0.580	1600	360	06	10	43.75	26 05 30.4	43.79	30.1	9	50.0*
0704 + 384	4C38.20	0.579	285	64	07	04	08.38	28 26 57.2	08.40	57.3	1	22.0
0736 - 019	3C185	1.033	346	40	07	36	02.34	-01 57 29.7	02.33	30.5	6	9.0*
0812 + 020	4C02.23	0.402	715	200	08	12	47.28	02 04 12.9	47.28	11.7	1	18.6*
0814 + 227	3C197	0.980	435	43	08	14	38.17	22 46 38.4	38.15	38.6	1	24.2*
0837 - 120	3C206	0.200	(245)	189	08	37	27.91	-12 03 54.4	27.96	53.9	1	174.0*
			1820	128								
0922 + 149	4C14.31	0.896	190	48	09	22	22.36	14 57 23.6	22.41	23.2	1	41.2
0927 + 362	3CR220.2	1.157	550	34	09	27	29.95	36 14 37.2	29.95	36.7	1	8.4
0937 + 391	4C39.27	0.618	130	8*	09	37	59.15	39 07 30.4	59.20	30.0	1	52.6*
0957 + 003	4C00.34	0.907	325	86	09	57	43.80	00 19 49.3	43.76	49.0	2	31.5*

1001 + 226	4C22.26	0.974	175 571	24 35	10 01	58.49	22 39	54.2	58.53	53.6	10	67.5
1004 + 130	4C13.41	0.240	(45) 915	24 33	10 04	45.04	13 03	36.9	45.05	37.7	1	100.0*
1012 + 022	4C02.30	1.374	245	43	10 12	40.80	02 13	49.9	40.80	49.3	3	8.5*
1015 + 277	3C240	0.469	405	15	10 15	00.34	27 47	05.4	00.42	05.6	11	21.7
1048 - 090	3C246	0.344	610 1920	60 35	10 48	59.40	-09 02	14.2	59.42	13.2	1	82.0
1058 + 110	4C10.30	0.420	235	5	10 58	10.73	11 02	20.6	10.80	19.4	1	33.9
1103 - 006	PKS	0.426	480	150	11 03	58.23	-00 36	38.7	58.24	38.8	8	21.6
1130 + 106	4C10.33	0.540	410	158	11 30	24.21	10 40	16.7	24.19	16.8	8	3.5*
1305 + 069	3C281	0.599	320	18	13 05	22.46	06 58	13.8	22.48	12.9	1	46.5
1335 - 061	PKS	0.625	995	22	13 35	31.17	-06 11	57.4	31.18	57.1	1	11.3*
1422 + 202	4C20.33	0.871	590	30	14 22	37.51	20 13	57.5	37.49	57.5	12	11.0*
1423 + 242	4C24.31	0.649	510	65	14 23	34.65	24 17	32.2	34.66	31.9	1	22.5
1530 + 137	4C13.55	0.771	370	35	15 30	54.22	13 42	27.8	54.29	28.3	8	11.8
1606 + 180	4C18.47	0.346	240	15	16 06	56.64	18 04	06.3	56.67	06.5	13	15.6*
1622 + 158	4C15.55	1.409	365	94	16 22	57.81	15 52	09.7	57.81	09.7	5	8.1
1623 + 269	4C26.48	0.779	190	*					11.50	13.3	14	5.5*
1634 + 269	3C342	0.561	400	9	16 34	34.26	26 54	10.0	34.22	10.0	1	39.7
2135 - 147	PKS	0.200	590 3450	126 117	21 35	01.17	-14 46	27.8	01.21	27.3	1	151.0*
2251 + 113	4C11.72	0.323	530	24	22 51	40.57	11 20	38.8	40.51	38.6	1	10.3
2252 + 129	3CR455	0.543	735						34.53	33.5	15	3.2
2349 + 327	4C32.69	0.659	(195) 735	24	23 49	48.93	32 47	17.9	48.94	18.3	10	60.0*

References to optical positions:

1. Miley & Hartsujker (1978); 2. Hintzen, Ulvestad & Owen (1983); 3. Wills, D. (1979); 4. Bolton *et al.* (1966); 5. Wills, B. J. (1976); 6. McEwan *et al.* (1975); 7. Argue & Kenworthy (1972); 8. Wills, Wills & Douglas (1973); 9. Riley & Pooley (1975); 10. Stannard & Neal (1977); 11. Fanti *et al.* (1975); 12. Argue, Kenworthy & Stewart (1973); 13. Ghigho (1977); 14. Potash & Wardle (1979); 15. Wills (1978).

Table 2. Contour maps of 45 quasars

Source	Rms value (mJy)	Peak value (mJy)	C (mJy)	Restoring beam		PA °
				Maj. axis "	Min. axis "	
0003 + 158	0.13	104.7	0.5	1.27	1.25	52
0118 + 034	0.15	26.5	0.6	1.36	1.24	-27
	0.35	121.8	1.0	4.20	3.90	18
0137 + 012	0.25	144.5	0.75	1.38	1.26	-25
	0.20	300.5	0.75	4.37	4.00	09
0158 + 183	0.10	145.6	0.5	1.19	1.13	-07
0159 - 117	0.42	770.9	2.0	1.65	1.14	05
0214 + 108	0.16	74.0	0.5	1.28	1.17	-03
	0.30	188.4	1.0	4.06	3.79	21
0222 - 008	0.1	269.3	0.4	1.37	1.21	00
0233 - 025	0.14	206.0	0.5	1.41	1.19	-02
0300 - 004	0.10	186.4	0.3	1.37	1.22	-08
0312 - 034	0.13	80.0	0.4	1.44	1.17	-06
0340 + 048	0.37	104.6	1.5	1.29	1.18	-14
0349 - 146	0.30	59.1	1.0	1.67	1.14	-19
	0.50	447.0	2.0	4.80	3.80	-30
0350 - 073	0.16	355.4	0.5	1.50	1.15	-10
0414 - 060	0.16	142.0	0.6	1.45	1.19	-15
0610 + 260	0.35	321.5	1.2	1.20	1.17	63
0704 + 384	0.11	62.6	0.3	1.17	1.12	-84
0736 - 019	0.13	189.4	0.4	1.45	1.29	-16
0812 + 020	0.13	187.8	0.4	1.31	1.27	-39
0814 + 227	0.18	240.4	0.5	1.31	1.27	-39
0837 - 120	0.21	172.3	0.75	1.31	1.16	-37
	0.45	120.9	2.0	5.18	3.67	-13
0922 + 149	0.12	54.1	0.4	1.65	1.27	-72
0927 + 362	0.15	222.0	1.0	1.47	1.08	79
0937 + 391	0.13	20.0	0.5	1.41	1.09	71
0957 + 003	0.09	84.0	0.3	1.31	1.25	-38
1001 + 226	0.10	32.2	0.3	1.57	1.23	-78
	0.22	159.3	0.75	4.30	4.20	-65
1004 + 130	0.17	23.6	0.5	1.70	1.40	-62
	0.75	44.1	2.0	4.31	4.24	-60
1012 + 022	0.09	133.7	0.3	1.29	1.26	-40
1015 + 277	0.12	231.9	0.4	1.39	1.18	-76
1048 - 090	0.26	159.4	1.0	1.41	1.20	-33
	0.50	531.9	2.0	4.47	3.92	-34
1058 + 110	0.09	39.4	0.3	1.28	1.24	-31
1103 - 006	0.13	137.0	0.4	1.41	1.25	-24
1130 + 106	0.09	166.2	0.3	1.29	1.24	-34
1305 + 069	0.12	53.6	0.4	1.27	1.22	-35

(Continued)

Table 2. (Continued)

Source	Rms value (mJy)	Peak value (mJy)	C (mJy)	Restoring beam		
				Maj. axis "	Min. axis "	PA °
1335 – 061	0.18	285.7	0.5	1.36	1.20	– 33
1422 + 202	0.12	261.6	0.4	1.41	1.24	– 73
1423 + 242	0.12	153.0	0.4	1.39	1.20	– 83
1530 + 137	0.10	128.1	0.4	1.81	1.37	– 64
1606 + 180	0.10	50.5	0.3	2.04	1.36	– 66
1622 + 158	0.10	146.1	0.5	2.22	1.41	– 63
1623 + 269	0.14	32.0	0.4	1.87	1.22	– 74
1634 + 269	0.10	236.0	0.4	1.86	1.21	– 73
2135 – 147	0.50	114.4	1.5	1.76	1.14	13
	1.00	587.9	3.0	5.42	3.62	10
2251 + 113	0.14	166.9	0.5	1.49	1.42	51
2252 + 129	0.35	349.7	1.0	1.49	1.33	58
2349 + 327	0.18	23.7	0.5	1.17	1.09	05
	0.26	71.7	0.75	3.62	3.46	33

- 1606 + 180:** Both the lobes appear to have tails oriented almost at right angles to the source axis.
- 1623 + 269:** Higher angular resolution is necessary to identify the radio core unambiguously. The radio structure appears to be significantly distorted and bent.
- 2135 – 147:** Our 20 cm map shows extended structure in the lobes (particularly the western lobe) oriented almost at right angles to the source axis.
- 2252 + 129:** Higher resolution is required to detect any possible radio core.
- 2349 + 327:** While there is a strong and almost continuous jet on the northwest side, part of a faint counter jet is seen on the southern side of the radio core.

Acknowledgement

I acknowledge the support of a US National Research Council – JPL Senior Research Associateship under which part of this research was carried out. The National Radio Astronomy Observatory and the VLA are operated by Associated Universities Inc., under contract with the National Science Foundation, USA.

References

- Argue, A. N., Kenworthy, C. M. 1972, *Mon. Not. R. astr. Soc* , **160**, 197.
- Argue, A. N., Kenworthy, C. M., Stewart, P. M. 1973, *Astrophys. Lett.*, **14**, 99.
- Barthel, P. D., Miley, G. K. 1988, *Nature*, **333**, 319.
- Barthel, P.D., Miley, G. K., Schilizzi, R.T., Lonsdale, C. J. 1988, *Astr. Astrophys. Suppl., Ser.*, **73**, 515.

- Bolton, J. G., Shimmins, A. J., Ekers, J., Kinman, T. D., Lamia, E., Wirtanen, C. A. 1966, *Astrophys. J.*, **144**, 1229.
- Fanti, C., Fanti, R., Ficarra, A., Formaggini, L., Giovannini, G., Lari, G, Padrielli, L. 1975, *Astr. Astrophys. Suppl.*, **19**, 143. 975.
- Ghigo, F. 1977, *Astrophys. J. Suppl.*, **35**, 359.
- Hewitt, A., Burbidge, G. 1993, *Astrophys. J. Suppl. Ser.*, **87**, 451.
- Hintzen, P., Ulvestad, J., Owen, F. 1983, *Astr. J.*, **88**, 709.
- Kapahi, V. K. 1987, in *Observational Cosmology*, Eds. A. Hewitt, G. Burbidge & L. Z. Fang (Dordrecht: D. Reidel) p. 252.
- Kapahi, V.K. 1990, *Curr. Sci.*, **59**, 561.
- Kapahi, V. K., Saikia, D. J. 1982, *J. Astrophys. Astr.*, **3**, 465.
- McEwan, N. J., Browne, I. W. A., Crowther, J. H. 1975, *Mem. R. astr. Soc.*, **80**, 1.
- Miley, G. K., Hartsuijker, A. 1978, *Astr. Astrophys. Suppl. Ser.*, **34**, 129.
- Orr, M. J. L., Browne, I. W. A. 1982, *Mon. Not. R. astr. Soc.*, **200**, 1067.
- Potash, R. I., Wardle, J. F. C. 1979, *Astr. J.*, **84**, 707.
- Price, R., Gower, A. C, Hutchings, J. B., Talon, S., Duncan, D., Ross, G. 1993, *Astrophys. J. Suppl. Ser.*, **86**, 365.
- Riley, J., Pooley, G. 1975, *Mon. Not. R. astr. Soc.*, **80**, 105.
- Singal, A.K. 1988, *Mon. Not. R. astr. Soc.*, **233**, 870.
- Stannard, D., Neal, D. 1977, *Mon. Not. R. astr. Soc.*, **179**, 719.
- Veron, M.P., Veron, P. 1989, *A Catalogue of Quasars and Active Nuclei* (4th Edition), ESO, Germany.
- Wills, B. J. 1976, *Astr. J.*, **81**, 1031.
- Wills, D. 1978, *Mon. Not. R. astr. Soc.*, **184**, 559.
- Wills, D. 1979, *Astrophys. J. Suppl.*, **39**, 291.
- Wills, B. J., Wills, D., Douglas, J. 1973, *Astr. J.*, **78**, 521.